

# **Photoacoustic Tomography Reconstruction And Classification**

T05995



**Muhammad Mohsin Riaz**

**87-FET/MSEE/F07**

This dissertation is submitted as partial fulfillment of degree

**MS Electronic Engineering**

**Department of Electronic Engineering**

**Faculty of Engineering and Technology**

**International Islamic University, Islamabad.**

**2009**



MS  
621.361  
R98  
C.1

Acc: TO5995

TO5995-C1V

TO6314 C2

Indiv  
MCA

Stoacoustic be Prothroscopy

Acoustic imaging

Tomography

Imaging systems in medicine

Not located in 315

## Certificate of Approval

It is certified that we have read the project report submitted by Muhammad Mohsin Riaz [87-FET/MSEE/F07]. It is our judgment that this project is of sufficient standard to warrant its acceptance by the International Islamic University, Islamabad for Master of Science Degree in Electronic Engineering.

**External Examiner**

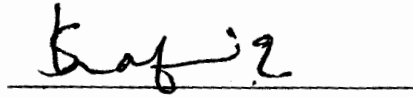
Dr. Abdul Jalil  
Associate Professor,  
PIEAS.



---

**Internal Examiner**

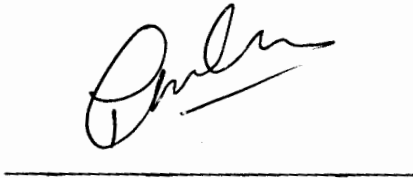
Dr. Mohammad Shafiq  
FET, IIU, Islamabad.



---

**Supervisor**

Dr. Tanweer Ahmad Cheema  
Assistant Professor,  
FET, IIU, Islamabad.



---

## Declaration

I certify that except where due acknowledgments has been made, the work is that of my alone: the work has not been submitted previously, in whole or in the part, to qualify for any other academic award; the content of the thesis is the result of work which has been carried out since the official commencement date of the approved research program; and, any editorial work, paid or unpaid, carried out by a third party is acknowledged.

A handwritten signature in black ink, reading "M Riaz Mohsin". The signature is written in a cursive style and is positioned above a horizontal line.

**Muhammad Mohsin Riaz**

87-FET/MSEE/F07

## Acknowledgements

In the name of Allah, the Most Gracious and the Most Merciful.

All praise and glory goes to Almighty Allah (Subhanahu Wa Ta'ala) Who gave me the courage and patience to carry out this research work. Peace and blessings of Allah be upon His last Prophet Muhammad (Sallulaho-Alaihihe-Wassalam) and all his Sahaba (Razi-Allaho-Anhum) who devoted their lives for the prosperity and spread of Islam.

First and foremost gratitude is due to the esteemed university, the International Islamic University Islamabad for my admittance. My deepest appreciation goes to my supervisor **Dr. Tanweer Ahmad Cheema** for his guidance and providing me the relevant material regarding thesis. He always helped me more than he can in my whole thesis. I would also like to thank my respected teacher **Dr. Ijaz Mansoor Qureshi** who always been a source of inspiration during my MS studies. My appreciation also goes to **Dr. Aqdas Naveed** for all his support during my thesis.

I extend my gratitude to all my close friends and university fellows who helped me a lot during my thesis. I am also thankful to all my other friends for their materialistic support and prayers. I would like to thank my beloved parents and family members. Their prayers and encouragement has always helped me to take the right steps in life.

May Allah help us in following Islam according to Quran and Sunna! (Aameen)



**Muhammad Mohsin Riaz**  
87-FET/MSEE/F07

## Abstract

Photoacoustic tomography (PAT) approach in medical imaging technique promises high quality imaging. PAT combines the contrast advantage of optical imaging technique and resolution advantage of ultrasonic imaging technique. Quality of reconstructed image in PAT directly depends on the reconstruction algorithm. Filtered Back projection (FBP) algorithm is used for image reconstruction if ultrasonic detector has ideal impulse response, while Deconvolution algorithm (DA) is used when the ultrasonic transducer has certain impulse response. Modified filtered back projection (mFBP) based on wavelet technique is implied in FBP and deconvolution algorithm for removing additive noise and enhancing image quality. PAT color quantization is performed for purpose of memory reduction and segmentation process using uniform color quantization, median cut color quantization and SOM(Self Organizing Maps) color quantization techniques. Two novel approaches are proposed for PAT image segmentation and classification based on single level edge detection and multilevel edge detection respectively. Performance and comparison of the proposed algorithms are evaluated based on Mean Square Error (MSE), Improved Signal to Noise Ratio (ISNR) and human visualization.

# TABLE OF CONTENTS

<b>Declaration</b>		<b>iii</b>
<b>Acknowledgements</b>		<b>iv</b>
<b>Abstract</b>		<b>v</b>
<b>List of figures</b>		<b>viii</b>
<b>List of tables</b>		<b>x</b>
<b>Acronyms</b>		<b>xi</b>
<b>1</b>	<b>Introduction.....</b>	<b>1</b>
	1.1 Contribution of the Dissertation.....	2
	1.2 Organization of the Dissertation.....	3
<b>2</b>	<b>Computed Tomography.....</b>	<b>4</b>
	2.1 Overview of Tomographic Imaging Techniques.....	4
	2.1.1 X-Ray Computed Tomography.....	5
	2.1.2 Magnetic Resonance Imaging.....	6
	2.1.3 Ultrasound or Ultra-Sonography.....	7
	2.1.4 Positron Emission Tomography.....	8
	2.1.5 Optical Coherence Tomography.....	8
	2.2 Photoacoustic Tomography.....	9
	2.2.1 Overview of PAT.....	9
	2.2.2 Block Diagram of PAT.....	11
	2.2.3 Absorption Rates.....	13
	2.2.4 Comparative analysis of PAT.....	14
	2.2.5 Applications of PAT in Biomedical.....	15
<b>3</b>	<b>PAT Image Reconstruction.....</b>	<b>17</b>
	3.1 Detection Techniques.....	17
	3.1.1 Focused Detection.....	18
	3.1.2 Unfocused Detection.....	18
	3.2 Reconstruction Types.....	18
	3.2.1 Approximate Reconstruction.....	19
	3.2.2 Exact Reconstruction.....	19
	3.2.3 Filtered Back Projection (FBP).....	20
	3.3 General Photoacoustic Equation.....	20
	3.3.1 Thermal Equation.....	20
	3.3.2 Basic Acoustic Equations.....	21
	3.4 Inverse Radon Transform.....	23
	3.5 Deconvolution Algorithm.....	29
	3.6 Modified Filtered Back Projection Algorithm.....	34
<b>4</b>	<b>PAT Image Classification.....</b>	<b>38</b>
	4.1 Color Quantization.....	39
	4.1.1 Uniform Color Quantization.....	39
	4.1.2 Median Cut Algorithm.....	40

4.1.3	Self Organizing Map.....	42
4.2	Segmentation.....	44
4.2.1	Edge Based Segmentation.....	44
4.2.2	Region based segmentation.....	48
4.2.3	Proposed Segmentation Technique.....	49
4.3	Proposed Classification Technique.....	50
<b>5</b>	<b>Simulation Results.....</b>	<b>54</b>
5.1	Image reconstruction in PAT.....	55
5.1.1	Inverse Radon Transform.....	56
5.1.2	Deconvolution Algorithm.....	58
5.1.3	Wavelet based Image Reconstruction.....	63
5.1.4	Comparison of Different Algorithms.....	67
5.2	Color Quantization Results.....	73
5.3	Results of Segmentation and Classification.....	76
5.3.1	Single level Segmentation and Classification.....	76
5.3.2	Multilevel Segmentation and Classification.....	78
<b>6</b>	<b>Conclusion and Future Directions.....</b>	<b>81</b>
6.1	Summary of Results.....	81
6.2	Future Directions.....	83
	<b>References.....</b>	<b>84</b>



## LIST OF FIGURES

Figure 2.1	Block diagram of PAT imaging acquisition system.	12
Figure 3.1	Frequency response of Ram-Lak Filter	25
Figure 3.2	Frequency response of Sinc window.	26
Figure 3.3	Frequency response Hamming window.	27
Figure 3.4	Frequency response of Hann window	28
Figure 3.5	Frequency response of Cosine window	29
Figure 3.6	Typical ultrasonic detector response	33
Figure 3.7	Haar Wavelet	36
Figure 3.8	Mexican Hat Wavelet	36
Figure 3.9	Morlet Wavelet	37
Figure 4.1	Median Cut Color Quantization Flow Diagram	41
Figure 4.2	SOM Color Quantization Flow Diagram	43
Figure 4.3	Different edge detector operators.	48
Figure 4.4	Flow diagram of Single level segmentation and classification algorithm (SLSC).	51
Figure 4.5	Flow diagram of Multi level segmentation and classification algorithm (MLSC).	53
Figure 5.1	Reconstruction using filtered back projection (FBP) algorithm.	57
Figure 5.2	MSE graph for inverse radon transform.	58
Figure 5.3	Reconstruction using Deconvolution algorithm (Channel Known).	59

Figure 5.4	MSE in deconvolution algorithm (Channel Known).	60
Figure 5.5	Reconstruction using Deconvolution algorithm (Channel Unknown).	61
Figure 5.6	MSE in deconvolution algorithm (Channel unknown).	62
Figure 5.7	Reconstruction using wavelet based FBP algorithm (mFBP).	63
Figure 5.8	MSE graph for modified wavelet based FBP algorithm.	64
Figure 5.9	Reconstruction using wavelet based Deconvolution algorithm (Channel Known).	65
Figure 5.10	MSE graph for wavelet based deconvolution algorithm (Channel Known).	66
Figure 5.11	Reconstruction using wavelet based Deconvolution algorithm (Channel Unknown).	67
Figure 5.12	MSE graph for wavelet based deconvolution algorithm (Channel Unknown).	68
Figure 5.13	MSE graph comparison for FBP and mFBP algorithm.	70
Figure 5.14	MSE graph comparison for FBP Deconvolution and wavelet based Deconvolution algorithm (Channel Known).	71
Figure 5.15	MSE graph comparison for FBP Deconvolution and wavelet based Deconvolution algorithm (Channel Unknown).	72
Figure 5.16	Results of Uniform color quantization technique.	73
Figure 5.17	Results of Median cut color quantization technique.	74
Figure 5.18	Results of SOM based color quantization technique.	75
Figure 5.19	Results of single level segmentation and classification technique (SLSC).	77
Figure 5.20	Results of multi level segmentation and classification technique (MLSC).	79

## LIST OF TABLES

Table 2.1	Comparison of different medical imaging techniques.	14
Table 5.1	MSE of reconstructed (using FBP) and original image.	57
Table 5.2	MSE of Deconvolution Algorithm for channel known.	60
Table 5.3	MSE of Deconvolution Algorithm for channel unknown.	62
Table 5.4	MSE of reconstructed (using mFBP) and original image.	64
Table 5.5	MSE of reconstructed Wavelet based deconvolution (channel known) mFBP algorithm.	66
Table 5.6	MSE of reconstructed image using Wavelet based deconvolution (Unknown) mFBP algorithm.	68
Table 5.7	ISNR of FBP and wavelet based mFBP.	69
Table 5.8	ISNR for FBP and mFBP Deconvolution Algorithm (Channel Known).	70
Table 5.9	ISNR for FBP and mFBP Deconvolution (Channel Unknown) Algorithm.	72
Table 5.10	MSE for different color quantization schemes.	75
Table 5.11	Average intensity of region and absolute difference with Mean of image.	77
Table 5.12	Average Intensity of region and absolute difference with mean of image.	79
Table 5.13	Average Intensity of region and absolute difference with Mean of image.	80

## Acronyms

CT	Computed Tomography
OCT	Optical Coherence Tomography
MRI	Magnetic Resonance Imaging
PAT	Photo Acoustic Tomography
US	Ultrasonography or Ultrasound
SOM	Self Organizing Maps
TAT	Thermo Acoustic Tomography
OAT	Opto Acoustic Tomography
AOT	Acousto Optical Tomography
DOT	Diffuse Optical Tomography
ANN	Artificial Neural Networks
PAM	Photoacoustic Microscopy
PAE	Photo Acoustic Effect
FBP	Filtered Back Projection
mFBP	Modified Filtered Back Projection
DA	Deconvolution Algorithm
RL	Ramachandran-Lakshiminyanan
SL	Shepp-Logan
MSE	Mean Square Error
SNR	Signal to Noise Ratio
ISNR	Improved Signal to Noise Ratio

SSE	Sum of Square Error
FFT	Fast Fourier Transform
IFFT	Inverse Fast Fourier Transform
KNN	Kohonen Neural Network
MCQ	Median Cut Quantization
UQ	Uniform Quantization
ROI	Region Of Interest
(SLSC)	Single Level Segmentation and Classification
(MLSC)	Multi Level Segmentation and Classification
PCC	Percentage of Correct Classification
dB	Decibel
GA	Genetic Algorithm
PSO	Particle Swarm Optimization

# **CHAPTER 1**

## **INTRODUCTION**

Photoacoustic imaging is a novel medical imaging technique based on Photoacoustic (PA) principal. It has the potential to study the interior organs of animals and human beings such as breast and brain with high contrast and high spatial resolution [1]. The goal of this technique is to combine the contrast advantage of the optical properties and resolution advantage of ultrasound. In Photoacoustic imaging, non ionizing laser pulses are delivered into biological tissues. Some of delivered energy will be absorbed and converted into heat leading to transient thermoelastic expansion which leads to wideband ultrasonic emission [2]. The generated ultrasonic waves are then detected by ultrasonic transducers and then the image is formed by reconstruction algorithms. The reconstruction can be done either in time or frequency domain by a variety of

reconstructive algorithms such as Deconvolution algorithm, Filtered Back Projection (FBP) algorithm and modified FBP based on wavelets [1][3]. In this thesis the above reconstructive algorithms will be evaluated for their performance on noise handling capabilities and time efficiency.

Segmentation and classification is a major field in the area of medical image analysis. Different segmentation techniques based on region properties and some based on edge detections were used for segmentation of medical imaging [4]. In this thesis new segmentation technique based on multilevel edge detection is presented. Classification is second major thing in medical image analysis. Classification is usually done for purpose of automatic ROI (Region on Interest) detection [4]. Novel ROI detection scheme is presented in this thesis that is based on average intensity difference.

## **1.1 Contribution of Dissertation**

This thesis contributes to the following fields.

- **Medical Imaging:** Photoacoustic tomography is widely used now a day in medical imaging. This thesis contributes towards the easy implementation of PAT as well as classification of medical imaging and automatic ROI detection.
- **Military Applications:** This thesis will also contribute towards the military applications associated with image processing and pattern recognition as well. New classification method proposed in this thesis can be used for automatic target detection and location estimation.

## **1.2 Organization of the Dissertation**

**Chapter 2: Computed Tomography:** This chapter can be divided in two major parts. First part explains the basic concepts of computed tomography and tomographic imaging techniques. In second part, brief overview of Photoacoustic tomography is discussed.

**Chapter 3: PAT Image Reconstruction:** This chapter deals with the image reconstruction/formation methods used in PAT. Detection schemes and overview of different reconstruction algorithms are also presented.

**Chapter 4: Segmentation and Classification in PAT:** This chapter deals with PAT image segmentation and classification. Major topics of this chapter are image quantization, segmentation and classification.

**Chapter 5: Simulation Results:** In this chapter, we will discuss our results obtained from the proposed algorithms presented in chapter 3 and 4.

**Chapter 6: Conclusion and Future Directions:** In this chapter, we summarized the results of proposed algorithm and possible future directions are also elaborated.



## **CHAPTER 2**

### **COMPUTED TOMOGRAPHY**

Tomography is an advance form of imaging, where three dimensional objects can be visualized slice by slice [2]. Computed tomography is an imaging technique in which a three dimensional image of a sample is constructed by computer from a series of plane cross-sectional images made along different axis. Different algorithms can be used for reconstruction of three dimensional structures from two dimensional data [4].

#### **2.1 Overview of Tomographic Imaging Techniques**

There are many medical imaging techniques that use the principle of tomography for image formation; some commonly known techniques are given as,

- X-Ray Computed Tomography

- Magnetic Resonance imaging
- Ultrasonography
- Positron Emission Tomography
- Optical coherence tomography

### **2.1.1 X-Ray Computed Tomography (CT)**

X-Ray Computed Tomography is commonly known as CT scanning, which uses ionized X-Ray radiation source to capture image of the body part of patient. X-Ray radiation is applied on a sample/organ and the resultant two dimensional data is collected by detectors at different angles. This two dimensional data is then combined by different algorithms to form three dimensional image of the sample/organ [2]. CT scanning is most common source of three dimensional data because X-Ray scanners are relatively inexpensive but the over doses of X-rays are hazardous to patients health. The major advantage of CT scanning is that it's inexpensive and relatively easy to implement as compare to other imaging techniques [2]. CT scanning has some drawbacks as well, like it uses high intensity X-ray that is harmful for human health. Moreover it is not as better in resolution and image quality as compare to other imaging technique. The working and structure of CT scanner is quite simple which consists of a couch and a circular gantry. First the patient is placed on the couch and then passed through the circular gantry. The source detector ring is rotated around the patient during the acquisition process of extracting a "slice" of data. The raw output from the detector array is back projected to form an image of the slice of the body.

### **2.1.2 Magnetic Resonance Imaging (MRI)**

A magnetic resonance imaging instrument uses powerful magnets to polarize and excite hydrogen nuclei in water molecules that lie in human tissue [2]. This produces spatially encoded detectable signal which results in images of the body. MRI usually uses strong electromagnetic fields and static magnetic field to polarize the hydrogen nuclei. Weaker time-varying electromagnetic fields known as gradient fields may also be used for spatial encoding. Moreover weak radio-frequency (RF) field can also be used for manipulation of the hydrogen nuclei and for the production of measurable signals, detected by using an RF antenna [2]. MRI like CT scanning creates 2D image of an organ of the body and is therefore, MRI is such medical technique that uses principle of tomographic imaging. MRI modern instruments are capable of producing high quality images in the form of 3D blocks, which in actual a generalization of the 2D tomographic concept.

MRI is not much associated with the health hazards like in other CT scanners as this technique does not uses of ionized radiation source for imaging. It is also observed that this technique did not have known long term effects of exposure to strong static field. As this technique is less dangerous to human health so limit on the number of scans using this technique can be vary from subject to subject. On the other hand maximum limit of X-ray CT scan are limited due to their health hazards. MRI uses RF fields as radiation source so there are some identified risks associated with health of tissues because RF fields produce heat which may be dangerous to tissue health [2]. The pressure of devices used in MRI may also produce slightly health hazards. These

risks may normally be controlled in the design phase of the instrument by using standard scanning protocols. MRI like CT scanning is also sensitive to different tissue properties. The appearance of the images obtained with the MRI and CT scanning is also different in visualization. The one of the major drawback of this technique is the psychological effects on the patient. The patient often feels the coldness and loneliness which closely resembles the effects of graves.

### **2.1.3 Ultrasound or Ultra-Sonography (US)**

Medical Ultra-Sonography uses high frequency sound waves (as radiation source) in the broadband Megahertz (MHz) range that are reflected by human body to produce two dimensional and three dimensional images. This imaging technique is commonly associated with imaging of the fetus in pregnant women [4]. Uses of ultrasound technology are much broader in range. The other important uses of ultrasound include imaging of the abdominal organs like heart, kidney, breast, liver, muscles, veins and arteries.

The ultrasound may provide less anatomical detail than other techniques such as CT scanning or MRI. However because of its several advantages, use of this technique in numerous situations is an ideal approach, such as study of the ultrasound of moving structures in real time. Ultrasound of moving structure normally contains speckle that may also be used in elastography. It does not appear to cause any adverse effects so this imaging technique may be very safe in use. It is also relatively inexpensive and quick in performance. Ultrasound scanners offer mobility. Therefore, the equipment of this imaging technique can be moved to intensive care units for imaging of

critically ill patients that avoids the possible danger may caused to patient by radiology department. The real time images obtained by ultrasound of moving objects may be used to guide the biopsy procedures. Doppler capabilities of modern ultrasound scanners also allow the assessment of the blood flow in arteries and veins [2].

#### **2.1.4 Positron Emission Tomography (PET)**

Positron emission tomography is commonly used to detect diseases related to the brain and heart. In PET a short lived isotope, such as  $^{18}\text{F}$ , is induced in to substance that is used by the human body such as glucose. The induced substance is absorbed by the tumor or region of interest similar to nuclear medicine [4]. PET scans are also a form of computed tomography technique, but PET imaging can be performed even without moving the patient by using special PET equipment.

#### **2.1.5 Optical Coherence Tomography (OCT)**

Optical coherence tomography (OCT) is an extremely high quality imaging technique that promises high resolution normally in micrometer. OCT uses optical energy as radiation source for signal acquisition. Processing method of this technique provides an edge other imaging technique that produces high quality two dimensional and three dimensional. In comparison with other imaging technique OCT uses an interferometric technique [2]. This imaging technique allows to, penetrate radiation source significantly deeper into human organs especially if the medium or organ is scattering in nature. OCT has already achieved sub micrometer resolution and the

research is in progress for even better resolution. OCT uses very wide-spectrum radiation sources normally in range of  $\sim 100$  nm. OCT normally uses super luminescent diodes or ultra-short pulse lasers for radiation [1]. Because of using high brightness and wide spectrum light sources this techniques holds good resolution properties. A relatively recent implementation of frequency-domain OCT provides significant advantages in terms of signal-to-noise ratio and faster signal acquisition.

## **2.2 Photoacoustic Tomography (PAT)**

*Photo* means light and *acoustic* means sound, in short *Photoacoustic* means the emission of sound waves from a material illuminated by a modulated light source [1]. The Photoacoustic effect forms the physical basis for Photoacoustic imaging; it refers to the generation of acoustic waves by the absorption of Electromagnetic or laser energy. Imaging depth and high resolution of this technique provides an edge over the past imaging techniques.

### **2.2.1 Overview of PAT**

Thermal expansion caused due to absorption of electromagnetic energy, results in production of acoustic waves. This PA effect can be used to image biological tissues in medical imaging [4]. Wide range of electromagnetic spectrum can be used to stimulate biological tissues for production of acoustic waves. Different biological tissues have different absorption rates on different frequencies/wavelengths [5][6]. Because of distinct penetration properties of tissues and different absorption rates for different wavelengths/frequencies, distinct EM laser pulse can also be used as

radiation source in PA imaging instead of RF pulse[5][7]. When laser pulse is implied the resultant system is called as TAT.

Motivation of PAT is to combine the contrast advantage of EM radiation and resolution advantage of ultrasound in biological tissues. Ultrasonic waves have (2-3 order of magnitude) weak scattering as compared to EM radiation so pure ultrasonic imaging provides better resolution in depths as compare to optical imaging.[2][8]. Ultrasound is not much useful in detection of early stage tumors, as it is based on the difference of mechanical properties of biological tissues. RF imaging normally uses long wavelengths that results in poor spatial resolution [9][10], while RF imaging provides better contrast as compare to ultrasonic imaging.

In PA imaging, maximum imaging depth and spatial resolution depends on radiation source and detectors. Ultrasonic detector determines image resolution, for example obtaining millimeter spatial resolution we should use mega hertz (MHz) ultrasonic transducer. Short wavelengths give better spatial resolution if used as radiation source in PAT [11]. PAT system may also be used to detect small embedded tumors with great sensitivity [6]. Detection of objects that are hidden in different layers of tissues is one of the most challenging problems in medical imaging. PAT has the ability to detect objects in layered tissue such as in skin [12]. The applications of PAT is not limited, it can also be used for imaging of blood vessels with high resolution [6]. Acoustic waves detected by ultrasonic transducer and two dimensional image can be reconstructed using some reconstruction algorithm. This provides the basic foundation of P.A imaging in two dimensions as well as in three dimensions.

Accurately detecting the acoustic waves by using ultrasonic transducer is one of the most challenging fields of research in PAT. More sensitive and sophisticated can provide better resolution and imaging depth [13]. The use of sector scanning and ring scanning in detection of ultrasonic signals promises better speed with comparable results. Image reconstruction and formation is also a very complicated and important task in PAT, better the reconstruction algorithm better the image formed [13]. Reconstruction in PAT is similar in nature with other tomographic techniques. Algorithms for X-ray tomography can be modified for PAT keeping in view the mathematical equations [11].

Exact reconstruction techniques in PAT provide much better results at the cost of efficiency and hardware complexity [11]. Reconstruction methods based on Fourier transform in PAT are comparatively easy to implement and promises good results. Time domain exact reconstruction in spherical geometry, planar geometry and cylindrical geometry can be used for reconstruction for getting best results at the cost of complexity in both time and hardware[14][15] . Moreover the complete information of scanning geometries should also be known for exact reconstruction.

### **2.2.2 Block diagram of PAT**

The general block diagram of Photoacoustic tomography (PAT) used for medical imaging is shown in Fig 2.1: [1].



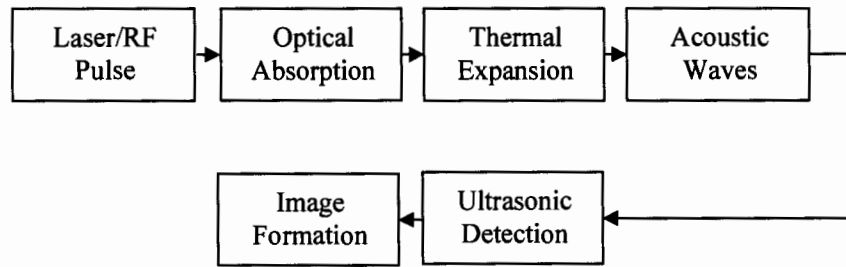


**Figure 2.1: The block diagram of PAT imaging acquisition**

**Laser/RF pulse:**

Laser or Radio Frequency (RF) electromagnetic pulse is used as input source. When laser pulse is used, the technique is called as Photo-Acoustic Tomography (PAT) or Opto-Acoustic Tomography (OAT). If the source is RF pulse the technique is called as Thermo-Acoustic Tomography (TAT).

**Optical absorption:**

The optical absorption is referred to as amount of light absorbed by the sample when laser pulse hits on the sample (to be processed). Some light energy scatters and the rest absorbs in the sample during this process. Amount of optical absorption depends on the laser/RF pulse used and the properties of the sample.

**Thermal Expansion:**

The phenomena of thermal expansion occur when optical energy absorbs in the sample. In other words, the energy absorbs in the sample as a result of optical absorption will appear in the form of thermal expansion.

**Acoustic Waves:**

An acoustic source is produced automatically in the sample as the result of thermal expansion. The acoustic source results in the production of wideband acoustic waves that are normally called as pressure waves or ultrasonic waves.

**Ultrasonic Detection:**

The pressure acoustic waves generated by the sample are detected by ultrasonic detectors. The detection can be performed in two modes i.e. forward mode or backward mode. In forward mode the laser irradiation is on one surface of sample and the ultrasonic detection is on the other surface of sample. While in backward mode the laser irradiation and the ultrasonic detection are on the same side/surface of sample.

**Image Formation/Image Reconstruction:**

The one dimensional data from ultrasonic detectors are used by different reconstruction algorithms for image formation. The image reconstruction methods are discussed in detail in sub sequent chapters.

**2.2.3 Absorption Rates**

Optical absorption in human tissues is closely associated with physiological properties such as oxygen saturation and hemoglobin concentration [6]. Optical absorption is different at different wavelengths in different tissues. Some tissues such as malignant tumors, melanin pigment lesions and blood vessels have obviously higher absorption

rates compared with surrounding tissues. For example the absorption contrast between breast tumors and normal breast tissues can be as high as 300% for 1064nm light. Similarly absorption contrast between the blood and the surrounding medium is around 1000% for 850nm light [5]. Absorption of optical energy and the relative emission of acoustic wave have always been an issue in design of any PAT system.

#### 2.2.4 Comparative analysis of PAT

Comparison of PAT with other modern imaging techniques is shown in table 2.1.

**Table 2.1: Comparison of different medical imaging techniques**

Properties	OCT	DOT	US	AOT/PAT
Contrast	Good	Excellent	Poor for early cancers	Excellent (=DOT)
Resolution	Excellent (~10 $\mu\text{m}$ )	Poor (~5 mm)	Excellent & Scalable (~150 $\mu\text{m}$ )	Excellent (=US)
Imaging Depth	Poor (~5 mm)	Excellent (~5 cm)	Good & Scalable (~3 cm)	Good & Scalable (=US)
Speckle Artifacts	Strong	None	Strong	None
Scattering Coefficient	Strong (~100/cm)	Strong (~100/cm)	Weak (~0.3/cm)	Weak

Some key advantages of PAT are listed below.

- High resolution in time and spatial domains.
- Imaging depth is high as compare to other imaging techniques.

## **2.2.5 Applications of PAT in Biomedical**

Photoacoustic tomography can be used in many applications. Three major and common applications in field of medical imaging are listed below [15].

### **1. Brain Lesion Detection**

Brain contains different types of tissues. Soft tissues refer to healthy tissues while hard tissue term is used for tumor or dead tissues. So in brain tissues with different optical absorption properties can be clearly identified. While in other imaging techniques, it's still a difficult job to detect brain lesions. More over immature or early stage tumor in brain can also be detected easily in PAT.

### **2. Hemodynamics Monitoring**

Hemodynamics monitoring means to monitor different properties of hemoglobin. For instance red blood cells, white blood cells and the other components of blood all have different absorption rates. By using PAT we can easily monitor the hemodynamics. For example the counting of red blood cells and white blood cells in any given region of interest can be easily done by using PAT imaging technique.

### **3. Breast Cancer Diagnosis**

It is quite difficult or even impossible in certain cases to detect early stage cancer by using conventional imaging techniques. PAT/TAT provides a wide margin in detection of early stage cancers, as cancer tissue and normal tissues have very different response to RF or laser pulse. Microwave pulse having low scattering is

usually used as excitation pulse for breast cancer diagnosis. Low scattering pulse is capable of penetrating thick (several cm) biological tissues with less than mm spatial resolution. A normal tissue in breast generates weak acoustic waves as compare to cancerous or dead tissues of breast that generates very strong acoustic waves when proper excitation is applied.

## **CHAPTER 3**

### **PAT IMAGE RECONSTRUCTION**

Image reconstruction in Photoacoustic tomography plays important role in PAT image analysis mostly in PAT image classification. The quality of image reconstruction depends on different entities like detection geometry, detector type and quality, reconstruction algorithm and noise reduction filters. A Reconstruction algorithm is one of the major factors that determine the quality of reconstructed image in PAT. There are different image formation/reconstruction methods which we will discuss in this chapter.

#### **3.1 Detection Techniques**

The quality of reconstructed image in PAT is directly dependent on detection scheme and reconstruction algorithm. Detection is referred to as the process of collecting

ultrasonic waves emitted from the sample as result of PA effect. Reconstruction in PAT is the process of image formation from different projections, i.e. data collected by ultrasonic detectors [1].

### **3.1.1 Focused Detection**

If focused ultrasound detector is used to acquire the photoacoustic signals; the detection method is referred to as focused detection [2]. Using focused detection technique for detection of acoustic waves then no reconstruction algorithm is required for image reconstruction, simply 2-D pint-by-point scanning forms 2-D image directly. Focused detection is commonly used in Photoacoustic Microscopy (PAM).

### **3.1.2 Unfocused Detection**

If unfocused ultrasonic detectors are used to acquire photoacoustic signals the detection technique is named as unfocused detection [2]. Using unfocused detection we need a reconstruction algorithm for inversely solving the photoacoustic equations. With focused detection we have limited/fixed imaging regions, while unfocused detection gives relatively broad/wide imaging regions.

## **3.2 Reconstruction Types**

Multiple detectors give different projections of PA source from different angles. These different projections are combined through a reconstruction algorithm. Reconstruction algorithms can be categorized as under [1].

### **3.2.1 Approximate Reconstruction**

Approximate reconstruction algorithm gives approximate solution of photoacoustic (PA) source. Approximate methods were normally used in early days of PA imaging technology. Examples of approximate reconstruction algorithm include [1][3][11].

- Weighted delay and sum method
- Optimal statistical approach
- Multi-element phase controlled technique
- Half time image reconstruction and etc

### **3.2.2 Exact Reconstruction**

Exact reconstruction algorithms give the exact solution of PA source. Exact reconstruction algorithms are different forms of universal back projection algorithm [15][16][17]. Examples include:

- Time domain reconstruction for thermo-acoustic tomography in spherical geometry
- Exact frequency domain reconstruction for thermo-acoustic tomography for planar geometry
- Exact frequency domain reconstruction for thermo-acoustic tomography for cylindrical geometry



### 3.2.3 Filtered Back Projection (FBP) (Approximate Reconstruction)

In Filtered Back Projection (FBP) reconstruction algorithm the different projections are first filtered and then combined through reconstruction algorithm for image formation. Filtering of projections removed unwanted components (normally noise and channel or impulse response) from data. Filtered back projection method based on rotation scanning configuration is a classical algorithm to reconstruct the cross sectional image [13][18][20]. Examples of these kinds of reconstruction method are

- Filtered Back Projection Algorithm (Inverse Radon Transform)
- Deconvolution Algorithm.
- Modified Filtered Back Projection (mFBP) Algorithm (wavelet based).

### 3.3 General Photoacoustic Equation

Mathematical model of PAT can be constructed using basic formulation of thermal and acoustic equations. Combination of above mention two methodologies in an elegant way results in Photoacoustic equations.

#### 3.3.1 Thermal Equation

Basic thermal equation that is frequently defined in thermodynamics literature is given as under,

$$\rho C_p \frac{\partial T(\vec{r}, t)}{\partial t} = H(\vec{r}, t) \quad (3.1)$$

Where the parameters are

$\rho$  = Density of material.

$C_p$  = Specific heat capacity of that material.

$T(r, t)$  = Temperature rise due to energy pumping pulse.

$H(r, t)$  = Heating function.

Heating function is defined as thermal energy per time and volume deposited by the energy source.

### 3.3.2 Basic Acoustic Equations

Acoustic phenomena can be given by the following acoustic waves.

$$\rho \frac{\partial^2}{\partial t^2} u(\bar{r}, t) = -\nabla p(\bar{r}, t) \quad (3.2)$$

$$\nabla u(\bar{r}, t) = -\frac{1}{\rho v^2} p(\bar{r}, t) + \beta T(\bar{r}, t) \quad (3.3)$$

where,

$v$  = Velocity of sound

$\beta$  = Isobaric Volume expansion coefficients

$u(r, t)$  = Acoustic displacement

$p(r, t)$  = Acoustic pressure

Taking  $\nabla$  on both sides of equation 2 we have.

$$\nabla \cdot \left( \rho \frac{\partial^2 u(\bar{r}, t)}{\partial t^2} \right) = -\nabla \cdot \nabla p(\bar{r}, t) \quad (3.4)$$

As  $\nabla$  is a liner operator so we have

$$\rho \frac{\partial^2}{\partial t^2} \nabla u(\bar{r}, t) = -\nabla^2 p(\bar{r}, t) \quad (3.5)$$

Putting value of  $\nabla u(r, t)$  from equation 3 we have

$$\rho \frac{\partial^2}{\partial t^2} \left[ -\frac{1}{\rho v^2} p(\bar{r}, t) + \beta T(\bar{r}, t) \right] = -\nabla^2 p(\bar{r}, t) \quad (3.6)$$

$$-\frac{1}{v^2} \frac{\partial^2}{\partial t^2} p(\bar{r}, t) + \beta \rho \frac{\partial^2}{\partial t^2} T(\bar{r}, t) = -\nabla^2 p(\bar{r}, t) \quad (3.7)$$

From equation 3.1 we have

$$\rho C_p \frac{\partial}{\partial t} T(\bar{r}, t) = H(\bar{r}, t) \quad (3.8)$$

Taking partial derivative  $\frac{\partial}{\partial t}$  on both sides we get

$$\frac{\partial}{\partial t} \left[ \rho C_p \frac{\partial}{\partial t} T(\bar{r}, t) \right] = \frac{\partial}{\partial t} H(\bar{r}, t) \quad (3.9)$$

$$\rho C_p \frac{\partial^2}{\partial t^2} T(\bar{r}, t) = \frac{\partial}{\partial t} H(\bar{r}, t) \quad (3.10)$$

$$\frac{\partial^2}{\partial t^2} T(\bar{r}, t) = \frac{1}{\rho C_p} \frac{\partial}{\partial t} H(\bar{r}, t) \quad (3.11)$$

Putting value in equation 3.4 we get

$$-\frac{1}{v^2} \frac{\partial^2}{\partial t^2} p(\bar{r}, t) + \frac{\beta \rho}{\rho C_p} \frac{\partial}{\partial t} H(\bar{r}, t) = -\nabla^2 p(\bar{r}, t) \quad (3.12)$$

$$\nabla^2 p(\bar{r}, t) - \frac{1}{v^2} \frac{\partial^2}{\partial t^2} p(\bar{r}, t) = -\frac{\beta}{C_p} \frac{\partial}{\partial t} H(\bar{r}, t) \quad (3.13)$$

The above equation is general photo-acoustic equation.

### 3.4 Inverse Radon Transform

Inverse radon transform is one of the simplest and earliest reconstruction algorithms in photo-acoustic tomography. As discussed earlier the acoustic data collected by the wide band ultrasonic transducers is integral of acoustic waves generated by many point sources as an effect of thermal expansion. Keeping in mind that impulse response of channel and ultrasonic transducers also affects the data along with additive noise that are unknown parameters in certain cases and somehow difficult to known. In above context, need of an algorithm arises that can work and form a good image without knowing the channel parameters.

Inverse radon transform algorithm states that acoustic data measured by ultrasonic transducers are simply viewed as radon transform of original acoustic data generated by sample so if we want to recover the original data we simple take inverse radon

transform of measured data. In other words we can say technically that the projections on the detectors are represented by integrals over spherical shells so mathematically we may express the said projections as under.

$$F(\bar{r}_o, t) = \frac{4\pi}{t} \int_0^t p_d(\bar{r}_o, t) dt = \int \int_{|r_o - r| = ct} p_o(\bar{r}) d\Omega \quad (3.14)$$

In above equation  $p_d(\bar{r}_o, t)$  is the actual acoustic data of point  $\bar{r}_o$  at time  $t$  and the measured data is  $F(\bar{r}_o, t)$ , we can see that the measured data is integral of actual acoustic data from different time. Our aim is to recover the actual acoustic signal  $p_d(\bar{r}_o, t)$  having received  $F(\bar{r}_o, t)$ . Based on above theory, Kruger and coworkers suggested back projection algorithm to reconstruct the original image [3]. Mathematically the algorithm can be expressed as under:

$$p_o(\bar{r}) = -\frac{1}{2\pi} \int_{S_o} \int \frac{dS_o}{r_o^2} \left[ t \frac{\partial p_d(\bar{r}_o, t)}{\partial t} + 2p_d(\bar{r}_o, t) \right]_{t = \frac{|r - r_o|}{c}} \quad (3.15)$$

Where,  $dS_o$  is the detector element at  $\bar{r}_o$ .

Inverse Radon transforms approximation works well for an object located near the center of the spherical (or circular) detection geometry. However, if the source deviates from center of the spherical geometry the results may get poor. So we can say that inverse radon transform limits its application in certain aspects. Another disadvantage of inverse radon transform is that as the number of projections increases for image formation the blurring artifacts become prominent in reconstructed image. Solution to this problem is filtering the projections prior to back projection, i.e. the

projections are first passed through a filter in frequency or time domain before back projection. Because of filtering the projections the inverse radon transform is also known as Filtered Back Projection (FBP) algorithm. Commonly used filters are given as under in frequency domain, one may calculate time domain version by taking IFFT.

### 1. Ram-Lak Filter

This filter is most commonly filter used in FBP algorithm. It is simply a ramp in frequency domain, mathematically,

$$H(\omega) = |\omega| \quad (3.16)$$

This filter is simple in nature and easy to implement with limited hardware. However the performance of this filter in terms of removing blurring artifact is not as good.

Figure 3.1: shows a typical Ram-Lak Filter in frequency domain.

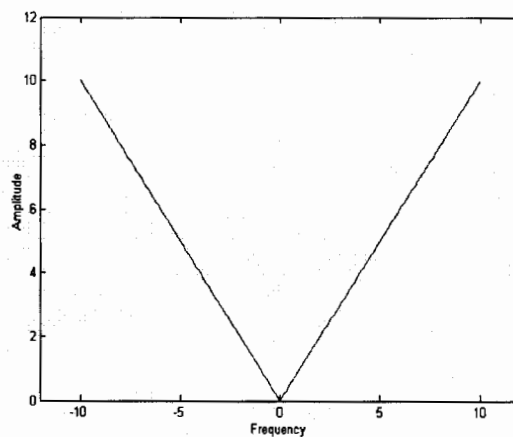


**Figure 3.1 : Ram-Lak Filter**

This filter is non-linear in nature, i.e. it suppresses low frequencies while enhancing high frequencies. Moreover this filter is very sensitive to noise. The maximum and minimum frequency of this filter can be limited according to application.

## 2. Shepp-Logan Filter

This filter is combination of Ram-Lak filter and Sinc Filter, i.e. if sinc function is multiplied with Ram-Lak filter in frequency domain we get Shepp-Logan filter.

Mathematically sinc function can be written as under:

$$H(\omega) = \text{sinc}(\omega) = \frac{\sin(\omega)}{\omega} \quad (3.17)$$

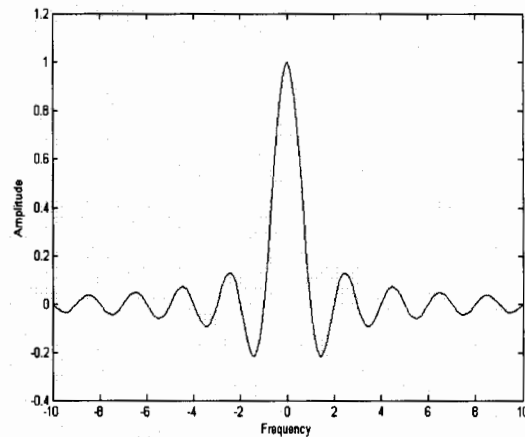


**Figure 3.2 : Sinc Function**

This filter gives better results as compare to Ram-Lak filter.

### 3. Hamming Filter

Hamming filter can also be used in FBP algorithm. This filter is simply the multiplication of Ram-Lak filter with Hamming window. Mathematically

$$H(\omega) = \begin{cases} a + (a-1) \cos \frac{2\pi\omega}{N-1} & 0 \leq \omega \leq (N-1) \\ 0 & \text{otherwise} \end{cases} \quad (3.18)$$

Where the constant ' $a$ ' can be used for choosing different windows (like hamming, hann) and ' $N$ ' represents the number of points in FFT i.e.  $N$ -point FFT. Hamming window can be obtained by setting value of constant ' $a=0.54$ ' that result in following equation

$$H(\omega) = \begin{cases} 0.54 - 0.46 \cos \frac{2\pi\omega}{N-1} & 0 \leq \omega \leq (N-1) \\ 0 & \text{otherwise} \end{cases} \quad (3.19)$$

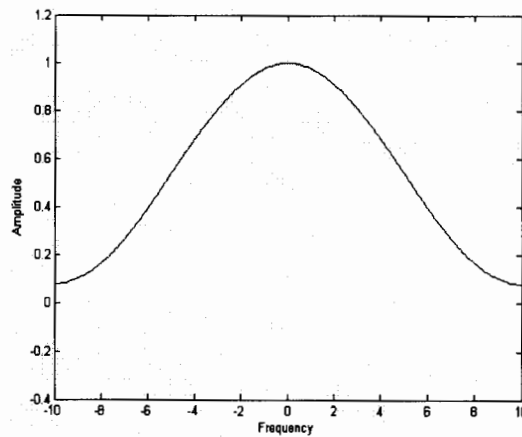


**Figure 3.3 : Hamming window**



The results of this filter are slightly better than Shepp Logan filter. If size of hamming window in frequency domain is not chosen correctly the results may become poor.

### 5. Hann Filter

Hann filter is multiplication of Ram-Lak Filter with Hann (Hanning) window. This filter gives best results in general cases of FBP algorithm. Hann window can be obtained by setting value of constant in equation 3. ' $a=0.5$ ', which result in following equation:

$$H(\omega) = \begin{cases} 0.5 - 0.5 \cos \frac{2\pi\omega}{N-1} & 0 \leq \omega \leq (N-1) \\ 0 & \textit{otherwise} \end{cases} \quad (3.20)$$

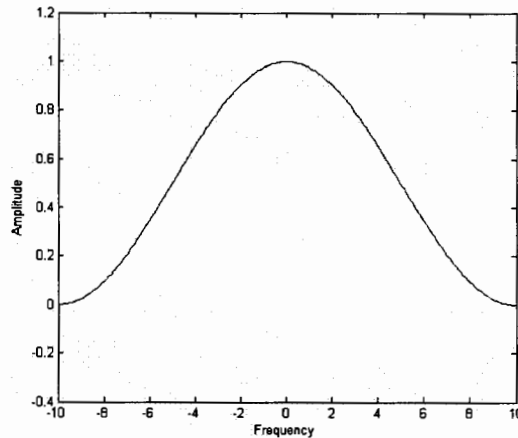


**Figure 3.4 : Hann window**

### 5. Cosine Filter

Cosine filter is multiplication of Ram-Lak filter with cosine filter in frequency domain. The equation of cosine window is given as under:

$$H(\omega) = \cos\left(\frac{\pi\omega}{N-1} - \frac{\pi}{2}\right) = \sin\left(\frac{\pi\omega}{N-1}\right) \quad (3.21)$$

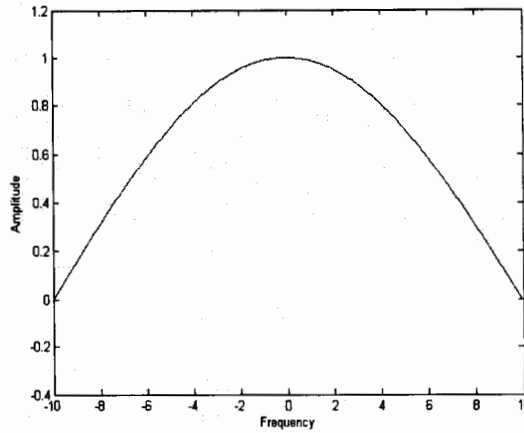


**Figure 3.5 : Cosine window**

This above filter is sometimes also known as Sine Filter or sine window.

### 3.5 Deconvolution Algorithm

Deconvolution algorithm is a reconstruction method that allows the optical absorption distribution of a sample to be constructed without knowing the impulse response of the ultrasonic transducer. A convolution relationship between photo-acoustic signals measured by an ultrasound transducer and optical absorption is developed. With conventional algorithms the impulse response of the ultrasonic transducer used for detection is crucial for PA imaging with high resolution and it is required for calculating induced PA pressures [3]. The basic photo-acoustic equation is given as

$$\nabla^2 p(\vec{r}, t) - \frac{1}{c^2} \frac{\partial^2}{\partial t^2} p(\vec{r}, t) = \frac{\beta}{C_p} \frac{d}{dt} H(\vec{r}, t) \quad (3.22)$$

Tit 5995

The solution of above equation can be found by Green's function as under

$$p(t) = \frac{\beta}{4\pi C_p} \iiint \frac{d\bar{r}}{r} \frac{\partial}{\partial t'} H(\bar{r}, t') \Big|_{t'=t-\frac{r}{c}} \quad (3.23)$$

Also we have

$$H(\bar{r}, t) = A(\bar{r})I(t) \quad (3.24)$$

Where A(r) and I(t) are spatial absorption distribution and temporal illumination function respectively.

So

$$H(\bar{r}, t') = A(\bar{r})I(t') \quad (3.25)$$

$$p(t) = \frac{\beta}{4\pi C_p} \iiint \frac{d\bar{r}}{r} \frac{\partial}{\partial t'} (A(\bar{r})I(t')) \Big|_{t'=t-\frac{r}{c}} \quad (3.26)$$

$$p(t) = \frac{\beta}{4\pi C_p} \iiint \frac{d\bar{r}}{r} A(\bar{r})I'(t') \Big|_{t'=t-\frac{r}{c}} \quad (3.27)$$

$$p(t) = \frac{\beta}{4\pi C_p} \iiint \frac{d\bar{r}}{r} A(\bar{r})I'(t-\frac{r}{c}) \quad (3.28)$$

In spherical coordinates we have

$$p(t) = \frac{\beta}{4\pi C_p} \iiint \frac{1}{r} A(r, \theta, \phi) I'(t-\frac{r}{c}) r^2 \sin(\theta) dr d\theta d\phi \quad (3.29)$$

Assuming  $t' = \frac{r}{c}$  the above equation can be written as

$$p(t) = \frac{\beta}{4\pi C_p} \int \left( \frac{1}{t'} \iint A(ct', \theta, \phi) (ct')^2 \sin(\theta) d\theta d\phi \right) I'(t-t') dt' \quad (3.30)$$

$$p(t) = \frac{\beta}{4\pi C_p} \left( \frac{1}{t} \iiint_{|\bar{r}|=ct} A(\bar{r}) dS \right) * I'(t) \quad (3.31)$$

Now it is proved earlier that typical response of typical PAT system can be written mathematically as [5]

$$p_0(t) = \frac{k}{r_p} I'(t) \quad (3.32)$$

Where k is the parameter depending on the absorption property of the point source and parameters of the irradiating light, and  $r_p$  is the distance between the point source and the field point. Form above equation we have

$$I'(t) = \frac{r_p}{k} p_0(t) \quad (3.33)$$

Putting the above value in previous equation we have

$$p(t) = \frac{\beta r_p}{4\pi C_p k} \left( \frac{1}{t} \iiint_{|\bar{r}|=ct} A(\bar{r}) dS \right) * p_0(t) \quad (3.34)$$

The recorded PA signals  $p_d(t)$  are the convolution of induced PA pressures  $p(t)$  and the impulse response  $h(t)$  of the transducer, we can write

$$p_d(t) = p(t) * h(t) \quad (3.35)$$

$$p_d(t) = p(t) = \frac{\beta r_p}{4\pi C_p k} \left( \frac{1}{t} \oint_{|\bar{r}|=ct} A(\bar{r}) dS \right) * p_0(t) * h(t) \quad (3.30)$$

$$p_d(t) = p(t) = \frac{\beta r_p}{4\pi C_p k} \left( \frac{1}{t} \oint_{|\bar{r}|=ct} A(\bar{r}) dS \right) * p_{d0}(t) \quad (3.36)$$

Where,  $p_{d0}(t) = p_0(t) * h(t)$ ,  $p_{d0}(t)$  denotes the recorded PA signal from point source, above equation can also be written as

$$\oint_{|\bar{r}|=ct} A(\bar{r}) dS = \frac{4\pi C_p k t}{\beta r_p} \text{IFFT} \left( \frac{P'_d(w)W(w)}{P'_{d0}(w)} \right) \quad (3.37)$$

Where  $P'_d(w)$  and  $P'_{d0}(w)$  are the Fourier transforms of  $p_d(t)$  and  $p_{d0}(t)$  respectively and  $W(w)$  is a window function used to band-limit the signals and taper the high frequency components smoothly to zero [3].

The projections of optical absorption distribution can be obtained by Deconvolution algorithm in the time domain. Optical distribution can be reconstructed using filtered back projection algorithm with sufficient number of projections acquired at different directions. The major advantage of Deconvolution algorithm is that we can easily measure  $p_{d0}(t)$  by focusing the incident laser on an absorber surface to form a point absorption source and thus eliminate the need for measuring the impulse response of the transducer [19]. Typical response of ultrasonic transducer can be shown by figure 3.6. The response on ultrasonic transducer may change accordingly to hardware

equipment but it is normally known or can be easily measured by focusing ultrasonic transducer or by using impulse response technique.

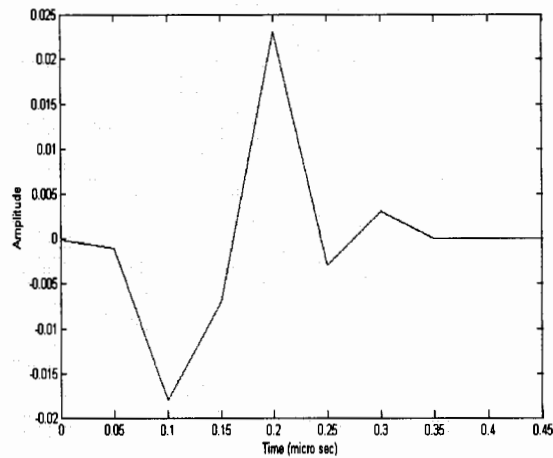


**Figure 3.6: Typical ultrasonic detector response**

The reconstruction by Deconvolution algorithm can be summarized by following steps:

- Calculating the projections of the optical absorption distribution by the equation derived above. This is normally done in two steps, i.e. in first step the emitted ultrasonic waves are detected and the response of detector is also measured and then by using the above equation we can easily measure the actual value of ultrasonic wave emitted by sample.
- Filtering the projections using the Shepp-Logan (SL) functions  $R(\omega) = |\omega(2\pi)| \text{sinc}(\omega)$  or by Ramachandran-Lakshminaryanan (RL) function.

- Back projecting it over spherical surfaces (3D) or arcs (2D). If the detection geometry is 2D then we back project it onto 2D surface and if the detection geometry is 3D or we can say in other words that if the detection is performed in some 3D domain then the back projection will be done in 3D surface.
- Summing or integrating the projections to form desired image in 2D or 3D.

### **3.6 Modified Filtered Back Projection Algorithm**

Modified filtered back projection algorithm is a method used for high quality image reconstruction that incorporates wavelet based analysis in filtered back projection algorithm. Wavelet analysis is normally applied for improving the quality of received signal. Its main purpose is to suppress noise as much as possible making the final reconstructed image quality as much better as possible.

In early sections we have discussed that in PAT the 1D data detected is actually radon transform of the original data emitted from sample. So we can recover our original data by keeping in mind the two major things. Firstly the channel response is known or channel is assumed to be ideal and noise variance is very low. Secondly the number of projections should be sufficient, i.e. more the projections quality of reconstructed will be better.

Wavelet based image reconstruction approach greatly helps in resolving the above two issues. Noise removal or noise reduction is naturally inherited characteristics of wavelets. One should keep in mind that the actual data collected by sensors is in continuous form with reference to time, so for processing that data with the help of

some digital machine like computers, the data has to be change in discrete form first that may results in some loss of information.

The basic wavelet transform equation is given as under:

$$T_{\varphi}(j_o, k) = \frac{1}{\sqrt{M}} \sum_n f(n) \varphi_{j_o, k}(n) \quad (3.38)$$

$$T_{\psi}(j, k) = \frac{1}{\sqrt{M}} \sum_n f(n) \psi_{j, k}(n) \quad \text{for } j \geq j_o \quad (3.39)$$

Where,  $f(n)$  represents the original function to be transformed,  $\varphi(n)$  represent the wavelet function and  $M$  is the total levels of wavelets. The inverse wavelet transform is written as under

$$f(n) = \frac{1}{\sqrt{M}} \sum_k T_{\varphi}(j_o, k) \varphi_{j_o, k}(n) + \frac{1}{\sqrt{M}} \sum_{j=j_o}^{\infty} \sum_k T_{\psi}(j, k) \psi_{j, k}(n) \quad (3.40)$$

Commonly used wavelets functions are given as under

### 1. Haar Wavelet

Haar is one of the basic wavelet functions used for wavelet transform. It is simple in nature and easily to implement. Mathematically:

$$\psi(n) = \begin{cases} +1 & 0 \leq n \leq 0.5 \\ -1 & 0.5 \leq n \leq 1 \end{cases} \quad (3.41)$$

Figure 3.7 shows a typical Haar wavelet function.



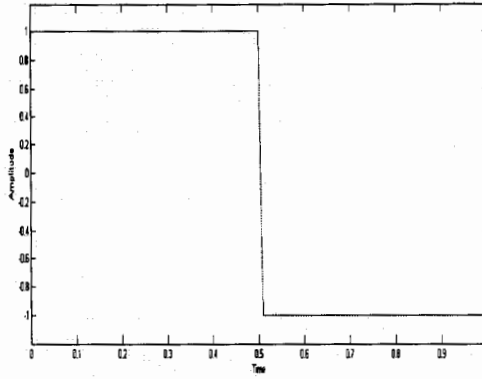


**Figure 3.7: Haar Wavelet**

## 2. Mexican Hat wavelet

Mexican Hat wavelet is another form of wavelet function that can be used for wavelet transform. It is continuous in nature but can be digitized. Mathematically,

$$\psi(n) = \left( \frac{2}{\sqrt{3}} \pi^{-1/4} \right) (1 - n^2) e^{-n^2/2} \quad (3.42)$$

Figure 3.8 shows a typical Mexican Hat wavelet function.

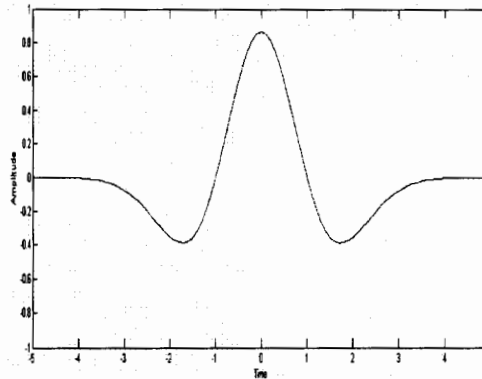


**Figure 3.8: Mexican Hat Wavelet**

### 3. Morlet wavelet

Morlet wavelet is one of most commonly wavelet function that can be used for wavelet transform. It is continuous in nature but can be digitized as necessary. It is also comparatively easy to implement and gives better results as compare to Mexican Hat wavelet. Mathematical form of Morlet wavelet function is given by equation 3.43.

$$\psi(n) = Ce^{-n^2/2} \cos(5n) \quad (3.43)$$

Figure 3.9 shows a typical Mexican Hat wavelet function.

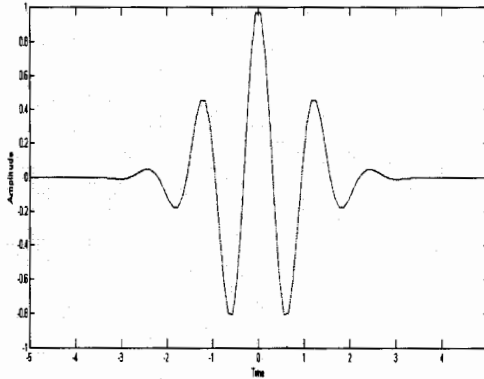


**Figure 3.9: Morlet Wavelet**

## **CHAPTER 4**

### **PAT IMAGE CLASSIFICATION**

PAT image classification refers to the problem of arranging data in two or more different classes on some given criterion. In medical imaging, the useful information that provides basics for classification criterion varies from case to case. In some cases the classification may be done between the detection of some abnormality like some fracture in a bone or a tumor in between healthy tissues. Other type of classification problem in medical imaging may be the classification of medical image on the basis of tumor structure and nature of tumor i.e. aggressive or non aggressive tumor. In this report, classification is used for dividing PAT images in two major categories i.e. tumor and non-tumor. Classification process can be divided in three following steps.

- Color quantization

- Segmentation
- Classification or ROI (Region Of Interest) detection

## **4.1 Color Quantization**

Color quantization is the process of reducing the total number of colors in any image. PAT imaging technique normally gives gray scale image as output having 256 shades between pure white and pure black. Color quantization in PAT is done for two major reasons. First by reducing total number of colors, this reduces the amount of memory required. For example, if the original image has 256 gray level shades then it requires 8 bits for storage of each pixel in the image. Now if the colors are reduced to 16 colors, only then only 4 bits are required for storage of each pixel. Second advantage of color quantization in PAT is that, when we have color quantized image the segmentation process becomes very simple and fast [4]. Another important aspect of color quantization is that decrease in number of colors will prominent the ROI. Hence, it becomes easy to extract the boundaries of ROI by any segmentation technique. There are many color quantization techniques some of them are listed below along with their brief description.

### **4.1.1. Uniform Color quantization**

Uniform color quantization is the simplest form of color quantization technique. The color space is quantized uniformly in this case, e.g. if we have a gray scale image having 256 colors and we want to quantize that image in 8, 16 or 32 colors, then we may divide the color space of 256 colors in 8,16 or 32 colors, respectively. In case of

4 colors, we may have the quantized colors as 0, 85, 170 and 255. This color quantization technique is very simple and fast in nature but it gives the worst results as compare to other quantization techniques [4]. In some special cases, when image histogram is not uniform this technique may gives bad results.

In PAT imaging the image histogram is usually not uniform in nature. May be the occurrence of white shades is more as compare to black once or vice versa. In PAT imaging if we apply uniform color quantization, the resultant image may be degraded to such a level where the actual information may get lost which we wanted to preserve. However, the time and processing complexity of this imaging technique is very low.

#### **4.1.2 Median Cut Quantization**

Median cut quantization is non-uniform quantization technique that promises better results as compare to uniform quantization technique. This technique is based on image histogram so no matter weather histogram is uniform or not this technique performs well. Basic principle of this technique is that, the resultant quantized image should represent equal number of pixel in that image. First the image histogram is calculated for original image. The histogram is divided from median in such a manner that the resultant both sides of histogram should have same number of pixels. The process continues in iterative fashion till we reach at the maximum allowable divisions of histogram. The mean or average value of each division is the color of that particular division. It can be observed that if we want to quantize an image in 8-colors than we must have 8-equal divisions of histogram.

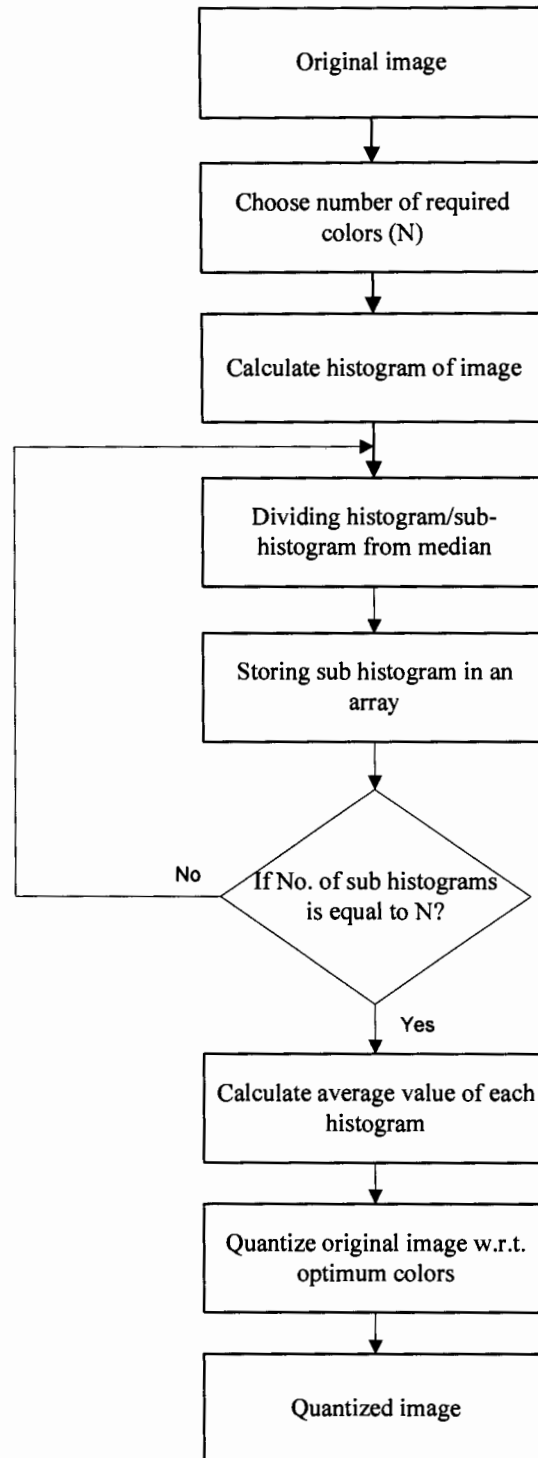


**Figure 4.1: Median Cut Color Quantization Flow Diagram**

Figure 4.1 shows the flow diagram of median cut color quantization algorithm. It can be observed that this technique is simple in nature and requires less execution time and hardware complexity as compare to SOM. Moreover, this technique provides much better results as compare of uniform quantization that may be comparable with other modern quantization technique like SOM or fuzzy quantization.

### 4.1.3 Self Organizing Map

Self organizing map (SOM) also known as Kohonen Neural Networks can also be used for color quantization and segmentation of PAT images. It is a neural network approach based on self learning technique. The implementation of this technique is quite simple and it guarantees optimal solution by minimizing the error. The weight updating equation of SOM is as under:

$$W(t+1) = W(t) + \eta(X - \hat{X}(t)) \quad (4.1)$$

The SOM works in a very elegant manner. Firstly the total number of optimum colors required after quantization. i.e. 8, 16 or 32 are selected. Initialization of optimum color vector can be done by some random values or by initial guess using a-priori information. Image is scan from left to right and top to bottom euclidian distances of each gray level in image and all the gray level in optimum color vector are calculated. The minimum distance is calculated from the list and optimum color vector is updated by equation 4.1. The above process is repeated until we get the best quantized colors. Finding optimum color vector quantize the original image with respect to optimum colors. Figure 4.2 shows the SOM color quantization flow diagram.

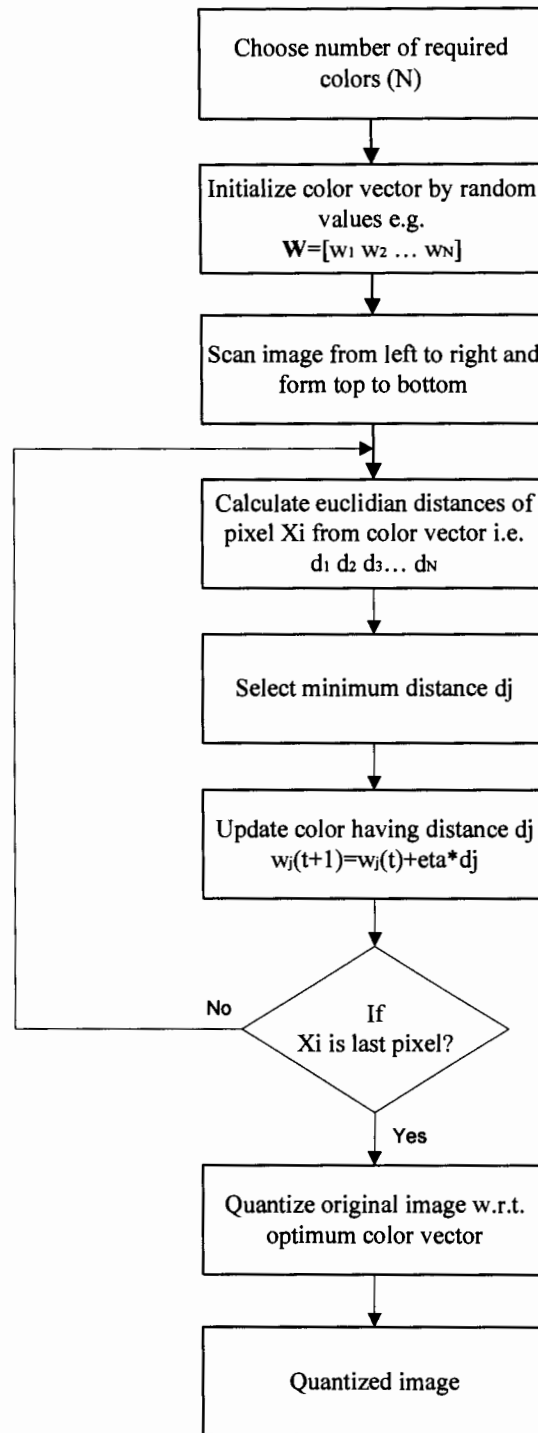


**Figure 4.2: SOM Color Quantization Flow Diagram**



## 4.2 Segmentation

Segmentation is the process of partitioning image into different segments based on some criteria. The basic aim of segmentation is to change an image in to another image such that the resultant image may become easy to view and analyze. Segmentation in PAT is normally done on brain tumor images for detection of tumor existence and its size estimation [4]. There are many segmentation techniques based on different learning methods but it can be divided into two major groups.

- Edge based segmentation
- Region based segmentation

### 4.2.1 Edge based segmentation

In this segmentation technique, firstly the edges of images are detected. Then on the basis of this information the segments and regions are defined in the original image. Edge detection can be done by many algorithms based on first order and second order derivative. Some of edge detection techniques can be given as under:

#### Robert Cross Edge Detection

In Robert cross edge detection the following kernels are applied on original image and the resultant image is edged image.

$$R_x = \begin{pmatrix} 1 & 0 \\ 0 & -1 \end{pmatrix} \text{ and } R_y = \begin{pmatrix} 0 & 1 \\ -1 & 0 \end{pmatrix} \quad (4.2)$$

Where  $R_x$  is used for detecting horizontal edges in images and  $R_y$  is used for detecting vertical edges in images as follow. If the image is represented by  $I$  then we have horizontal and vertical edges as under:

$$E_x = R_x * I \text{ And } E_y = R_y * I \quad (4.3)$$

The average edge image  $E$  can be calculated as under

$$|E| = \sqrt{E_x^2 + E_y^2} \text{ and } \theta = \tan^{-1} \left( \frac{E_y}{E_x} \right) \quad (4.4)$$

### Sobel Edge Detection

Detection of edges using sobel operators, the following kernel should be applied on the image.

$$S_x = \begin{pmatrix} -1 & 0 & 1 \\ -2 & 0 & 2 \\ -1 & 0 & 1 \end{pmatrix} \text{ and } S_y = \begin{pmatrix} 1 & 2 & 1 \\ 0 & 0 & 0 \\ -1 & -2 & -1 \end{pmatrix} \quad (4.5)$$

Where  $S_x$  is used for detecting horizontal edges in images and  $S_y$  is used for detecting vertical edges in images as follow. If the image is  $I$  then we have horizontal and vertical edges as under

$$E_x = S_x * I \text{ And } E_y = S_y * I \quad (4.6)$$

The average edge image  $E$  can be calculated as under

$$|E| = \sqrt{E_x^2 + E_y^2} \text{ and } \theta = \tan^{-1}\left(\frac{E_y}{E_x}\right) \quad (4.7)$$

### Prewitt Edge Detection

Detecting of edges using sobel operator, the following kernel should be applied on the image.

$$P_x = \begin{pmatrix} -1 & 0 & 1 \\ -1 & 0 & 1 \\ -1 & 0 & 1 \end{pmatrix} \text{ and } P_y = \begin{pmatrix} 1 & 1 & 1 \\ 0 & 0 & 0 \\ -1 & -1 & -1 \end{pmatrix} \quad (4.8)$$

Where  $P_x$  is used for detecting horizontal edges in images and  $P_y$  is used for detecting vertical edges in images as follow. If the image is represented by  $I$  then we have horizontal and vertical edges as under

$$E_x = P_x * I \text{ And } E_y = P_y * I \quad (4.9)$$

The average edge image  $E$  can be calculated as under

$$|E| = \sqrt{E_x^2 + E_y^2} \text{ and } \theta = \tan^{-1}\left(\frac{E_y}{E_x}\right) \quad (4.10)$$

### Canny Edge Detection

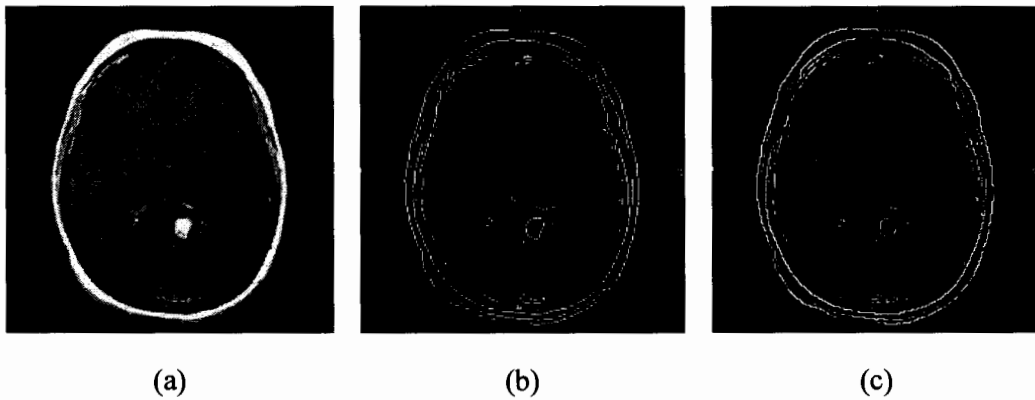
Canny edge detection basically works in following two steps

- **Step 1:** A Gaussian kernel is first applied on image to remove false edges and noise. The greater the size of Gaussian kernel the smoother the resultant image. If

the resultant image is much smoother (due to large size of kernel) then some useful edges may be lost in this technique. If the kernel size is small then the resultant image after applying Gaussian kernel is not much smooth then some false edges, due to noise or other image imperfections, may be detected in the second step of this detection scheme.

- **Step 2:** In second step we have Gaussian distributed smooth image as input, then edge detection can be performed using any of above operator like, Sobel, Prewitt or Robert Cross operator. The magnitude and direction of edges can be measured in the same manner.

Canny's edge detection algorithm is computationally more expensive compared to Sobel, Prewitt and Robert's operator but it provides the best results. Figure 4.1 shows the results of different edge detector operators. As shown in Fig 4.3 (e) the canny edge detector works in an elegant method that removes the false edges and preserves the original edges of the image.



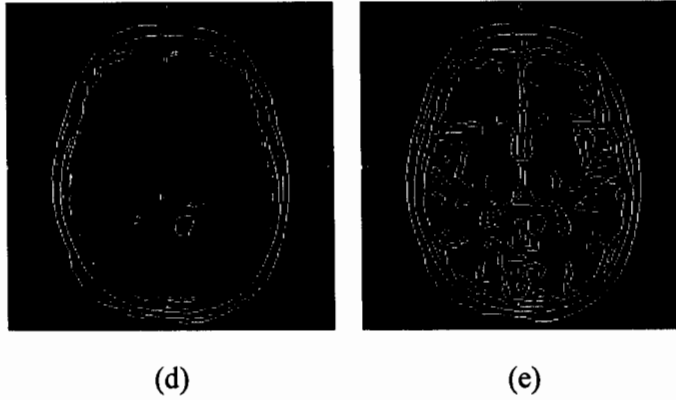


**Figure 4.3: (a) Original image. (b) Robert Cross edge detection (c) Sobel edge detection (d) Prewitt edge detection (e) Canny edge detection.**

#### **4.2.2 Region based segmentation**

Region based segmentation can also be used for segmentation of images. There are many algorithms for segmentations which are based on region based technique. The main idea in region based segmentation is to select any pixel in the image and check for its neighbor pixels that weather the neighbor pixels have almost same intensity as observed pixel. A threshold is normally set for this purpose. For example threshold of 20 can be set in gray scale image having 256 colors that if the distance of current pixel intensity with neighboring pixel intensity is less than 20 than both pixel belong to same segment or region else the neighboring pixel belong to some other segment.

The region based segmentation can be done using different approaches like

- Similarity matching
- Original seed pixel matching
- Neighbor in region matching

- Region statistics matching

There are much more approaches that can be used in region based segmentation methods. Some commonly used segmentation techniques based on region based method are “k-means clustering” and “Region growing segmentation”.

### **4.2.3 Proposed Segmentation Technique**

Segmentation based on multilevel edge detection has been proposed. Multilevel edge detection technique implies that the edges of same image are detected at multi-resolution or multi levels. The idea of multi level edge detection is generated from wavelet analysis in which images are viewed at different levels for the purpose of getting maximum information from the same data. Some information in images is available at high resolution and some other information may be at low resolution.

Segmentation using multi resolution implies that firstly, the edges of images are detected on original size of image and closed medium size edges are kept for segmentation purpose. Then the image is scale down to 9/10 resolution. Same procedure as above is done and the resultant closed medium size edges are scaled up to the original size images. Similarly, for resolution of 8/10, 7/10, 6/10 and 5/10 or even on less resolution as required in the application the above procedure is applied. At resolution of 5/10, we actually have image of half size as compare to original image. Canny edge detector is used as edge detector operator in proposed algorithm for its ability to detect edges accurately and removing false edges. Efficiency and performance of above proposed technique is measured for different medical images,

specifically on PAT images. Excellent results have been obtained by this technique but somehow time efficiency and hardware complexity may increase for multi levels.

### **4.3 Proposed Classification Technique**

Novel algorithm for classification is proposed in this section for automatic tumor or ROI (Region of Interest) detection. This algorithm is simple in nature and very easy in implementation. Previous classification algorithms have been case sensitive depending on the nature of data to be processed. Some algorithms give acceptable results at the cost of high processing time and hardware cost.

Working of this algorithm can be explained in few lines. Firstly the original gray level image is being loaded. Then median filter of size 9x9 is applied on original image for smoothing purpose. Edges of the smoother image are detected by applying canny edge detector. Subtraction of small and very large edges from above edged image because edge image normally contains many extra edges that are useless in detection of ROI. Now search for close edges in the image. Process of finding close edges can be done by using neighboring information from each pixel. Remove all the other edges and only retaining the close edges. Fill those close edges with the original values in median filtered image. Calculate the average intensity values of all the close edges separately, i.e. if we have 5 close edges then there are 5 average intensity values corresponding to each close segment. Calculate the average intensity of entire whole image. Calculate the absolute intensity difference between average intensity of entire image and the other close region. The region having maximum absolute difference will be our required ROI.

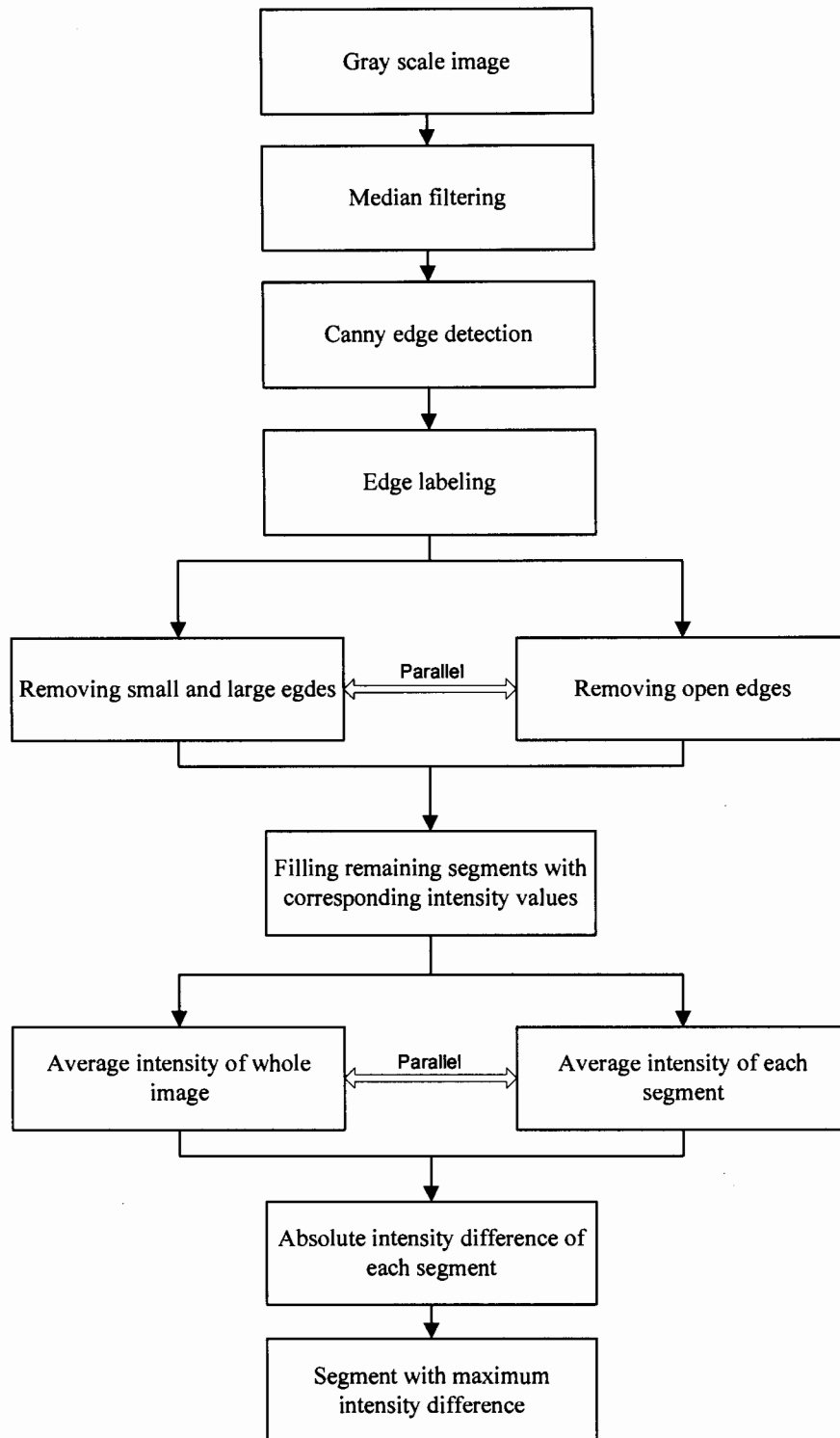


**Figure 4.4: Flow diagram of Single level segmentation and classification algorithm.**



This idea of above algorithm is based on the fact that normally the tumor or other ROI have different intensity range as compare to whole image. For example in brain MRI or PAT imaging if there exists some tumor the shape of tumor is closed and its intensity values are much different from the whole image. If whole image intensity is nearly white then the blood vessels or tumor have intensity near in black region because of PAT basic principle. This technique is very simple in nature but its accuracy rate is much high. In above algorithm the small and very large edges are removed because the ROI is normally not so much small or so much large in nature. Making the threshold value of large edges high and small edges very small we can retain almost all the edges in the images. The more closer the upper and lower bounds the less medium size edges we have at the output that results in less computation, complexity and processing time. Figure 4.4 shows the flow diagram for proposed single level segmentation and classification (SLSC) technique. Some process can be done in parallel fashion that makes the proposed technique efficient in processing. Steps are easy to understand and can be implement at minimal cost of time and complexity. Figure 4.5 shows the flow diagram of multilevel segmentation and classification technique. The proposed algorithm can be implemented using parallel processing techniques for the sake of fast processing. MLSC technique is time inefficient but more accurate as compare to SLSC technique.

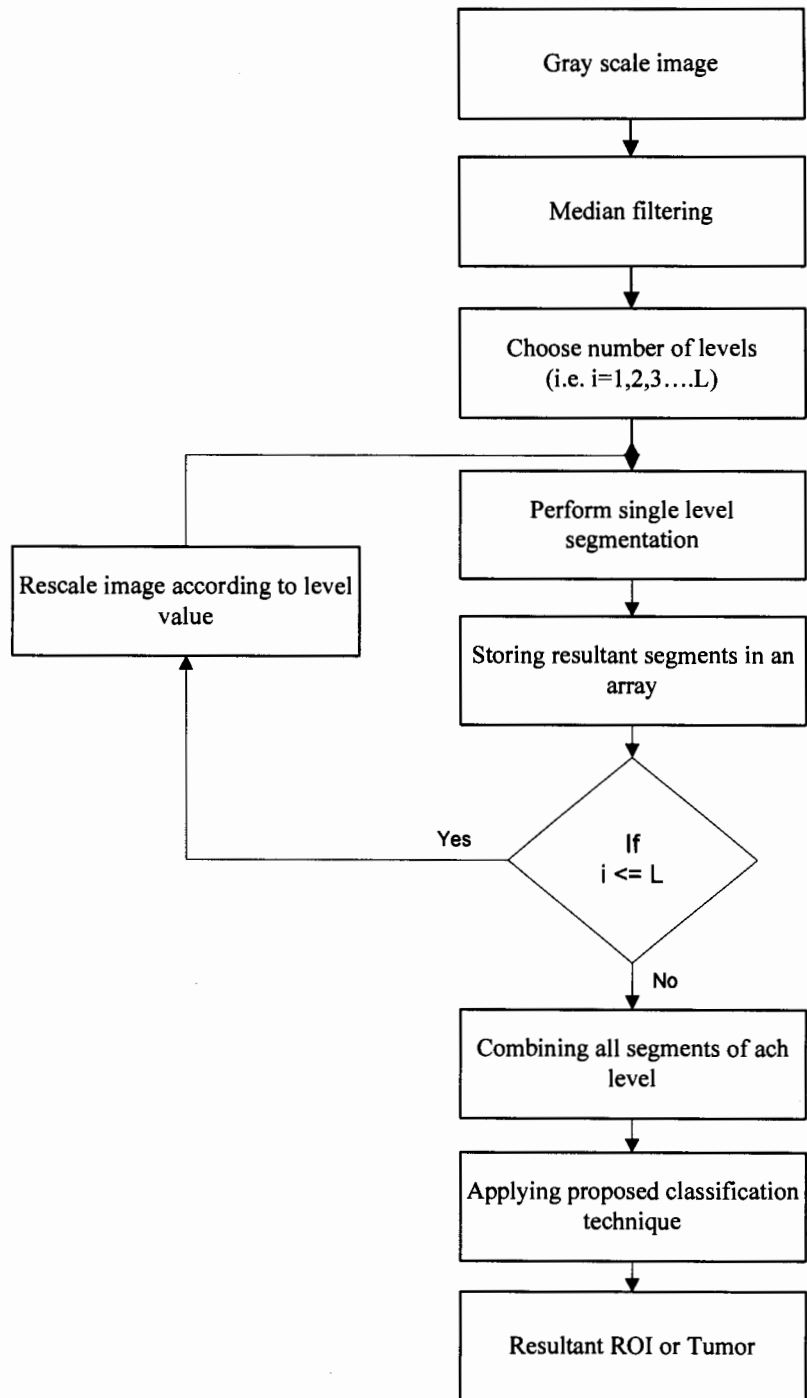


**Figure 4.5: Flow diagram of Multi level segmentation and classification algorithm.**

## **CHAPTER 5**

### **SIMULATION RESULTS**

The results for PAT image reconstruction and classification are shown in this chapter. Original PAT images are first transformed using radon transform that gives the projections of original image. These projections are passed through AWGN channel of various SNR for filtered back projection algorithm. The distorted signals are passed through filter for removing blur artifacts, than these projections are back projected to get original image. In Deconvolution algorithm the projections are first convoluted with the typical response of ultrasonic transducer in time domain. Resultant projections are passed through AWGN having various SNR. In Modified filtered back projection algorithm the projections are convoluted and passed through AWGN and deconvoluted in same manner as earlier but the resultant projections are enhanced using wavelet analysis before applying filtered back projection algorithm.

For PAT image classification, the image is first filtered using median filtering. The filter mask size may increase or decrease depending on image quality and type of information we want to extract from it. This pre filtering is done for removing certain noise in image and to making image smooth for better extraction of segments. Image quantization using uniform quantization technique and SOM (Self Organizing Maps) is also shown graphically and in tabular form. The result of single level segmentation is first verified and later on results of multilevel segmentation is also shown for comparison.

Three different criterion are being used for checking performance of these algorithms i.e. MSE (Mean Square Error), ISNR (Improved Signal to Noise Ratio) and human visualization. Different one dimension projections are used for construction of two dimension data, so as the number of projections increases the quality of image increase in both three performance criterion.

## **5.1 Image Reconstruction in PAT**

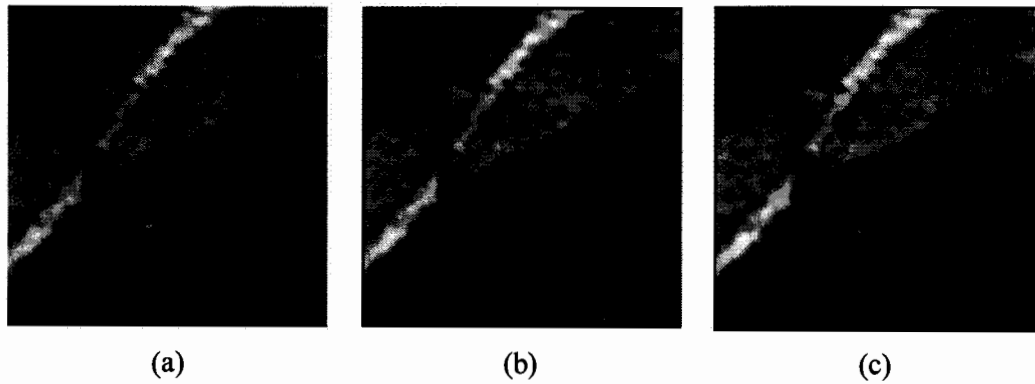
Results for PAT image reconstruction for different algorithms are verified for different parameter values. Three main algorithms are used for image reconstruction in PAT. PAT image reconstruction using inverse radon transform is shown first assuming the response of ultrasonic transducer (response of channel) to be ideal. The inverse radon transform is very simple, fast and good reconstruction algorithm if additive noise is also assumed to be a single constant or zero. Results of image reconstruction using different filters (*Ram-Lak*, *Shepp-Logan*, *Cosine*, *Hamming* and *Hann*) in inverse radon transform technique are also presented in table for different

values of angle separation. Two figures of merits are shown that are visualization and MSE as discussed earlier.

In second section the results of Deconvolution algorithm is shown for two variants i.e. if response of ultrasonic transducer is completely known and then for completely unknown respectively. A typical response of ultrasonic transducer is also shown. As discussed earlier in chapter 3 that Deconvolution algorithm works in two main steps i.e. deconvoluting the signal and then back projecting the signal using inverse radon transform. Modified filtered back projection algorithm first enhance the signal using wavelet analysis and then using filtered back projection algorithm it back project the data to form internal structure using external projections.

### 5.1.1 Inverse Radon Transform

Reconstruction using inverse radon transform using Ram-Lak filter in absent of any channel (i.e. channel is assumed to ideal) is given by following figures:



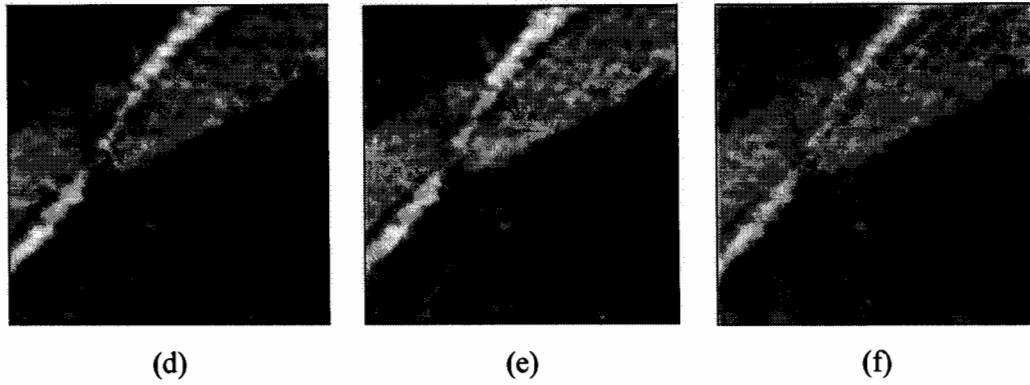


**Figure 5.1: (a) Original PAT image for filtered back projection (FBP) algorithm (b) Reconstruction using 180 projections (c) Reconstruction using 90 projections (d) Reconstruction using 60 projections (e) Reconstruction using 45 projections (f) Reconstruction using 36 projections.**

Having maximum number of points we can have better reconstruction using inverse radon transform. Table 5.1 shows the MSE for different types of filters and for different number of projections.

**Table 5.1: MSE of reconstructed (using FBP) and original image**

<b>Filter</b>	<b>Theta=1</b>	<b>Theta=2</b>	<b>Theta=3</b>	<b>Theta=4</b>	<b>Theta=5</b>
<b>Ram-Lak</b>	0.1158	0.1519	0.1569	0.1575	0.1611
<b>Shepp logan</b>	0.0997	0.1512	0.1575	0.158	0.162
<b>Cosine</b>	0.0657	0.1251	0.1353	0.1373	0.1462
<b>Hamming</b>	0.0521	0.1035	0.1217	0.1249	0.1324
<b>Hann</b>	0.0453	0.0924	0.1101	0.1128	0.1191

Figure 5.2 shows the graph of MSE versus angle separation for different filters in inverse radon transform algorithm. It can be seen from above said graph that as the

number of angle increases (or in other words angle separation decreases) the MSE decreases. It can also be observed by the figure that Hann filter gives better results as compare to other filters in terms of MSE. The graph has steep slope below angle separation of 5 degree.

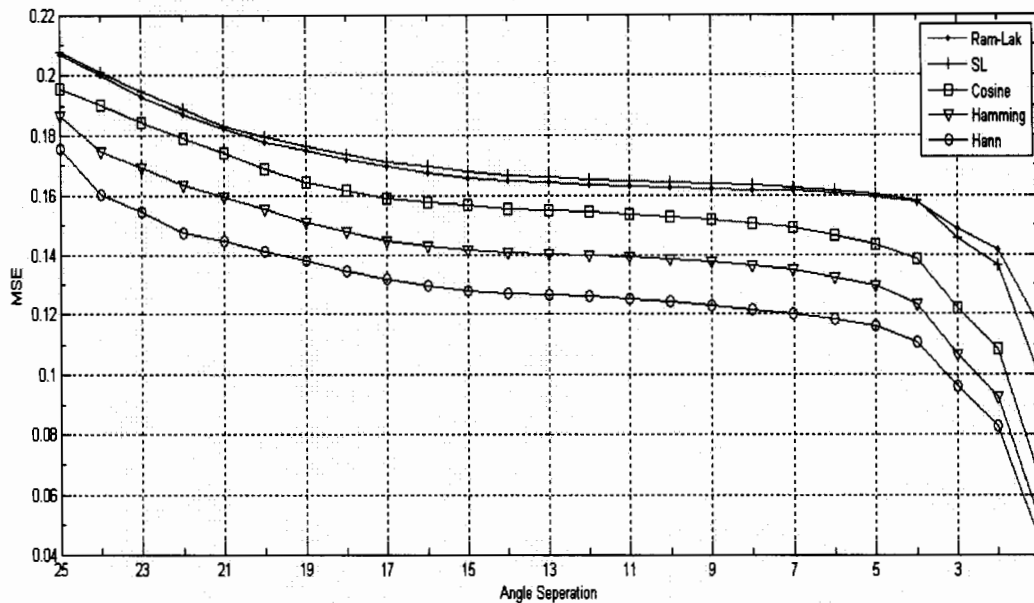


**Figure 5.2: Mean Square Error (MSE) versus Angle separation for different filters for inverse radon transform.**

### 5.1.2 Deconvolution Algorithm

Results of deconvolution algorithm are presented in this section. Figure 5.2 shows the results for deconvolution algorithm if the channel response is completely known and the additive white Gaussian noise (AWGN) is unknown having zero mean. Signal to noise ratio (SNR) is kept here at 20dB. As SNR decreases the results become poor even if the channel response is kept constant and vice versa.

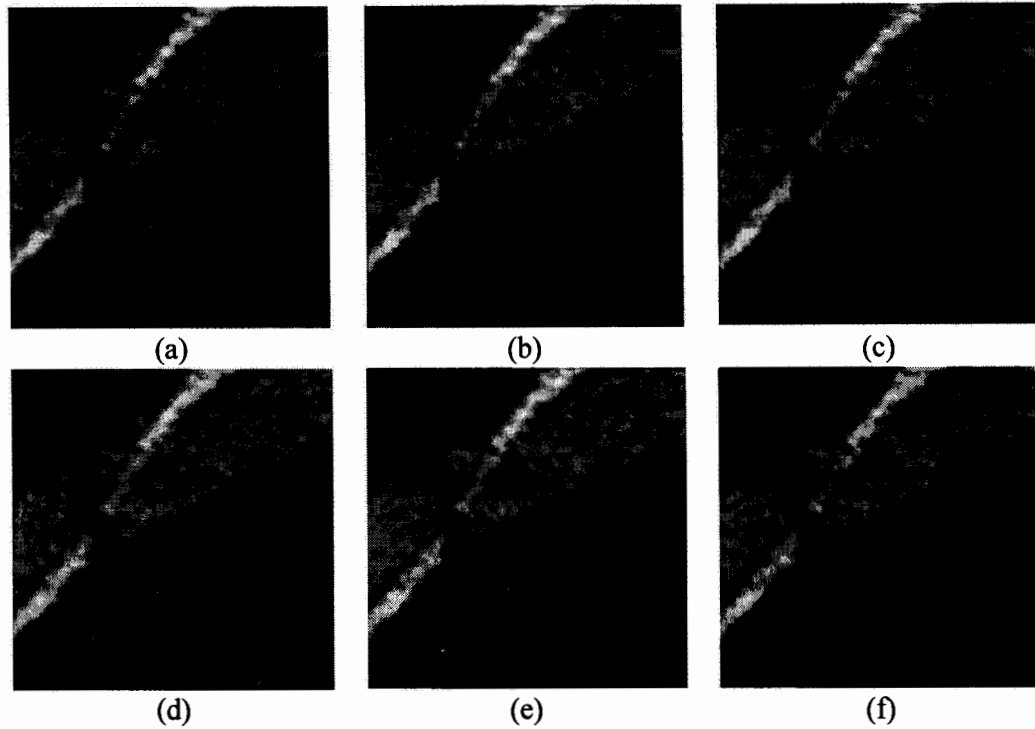


**Figure 5.3: (a) Original image for Deconvolution algorithm (Channel Known) (b) Reconstruction using 180 projections (c) Reconstruction using 90 projections (d) Reconstruction using 60 projections (e) Reconstruction using 45 projections (f) Reconstruction using 36 projections.**

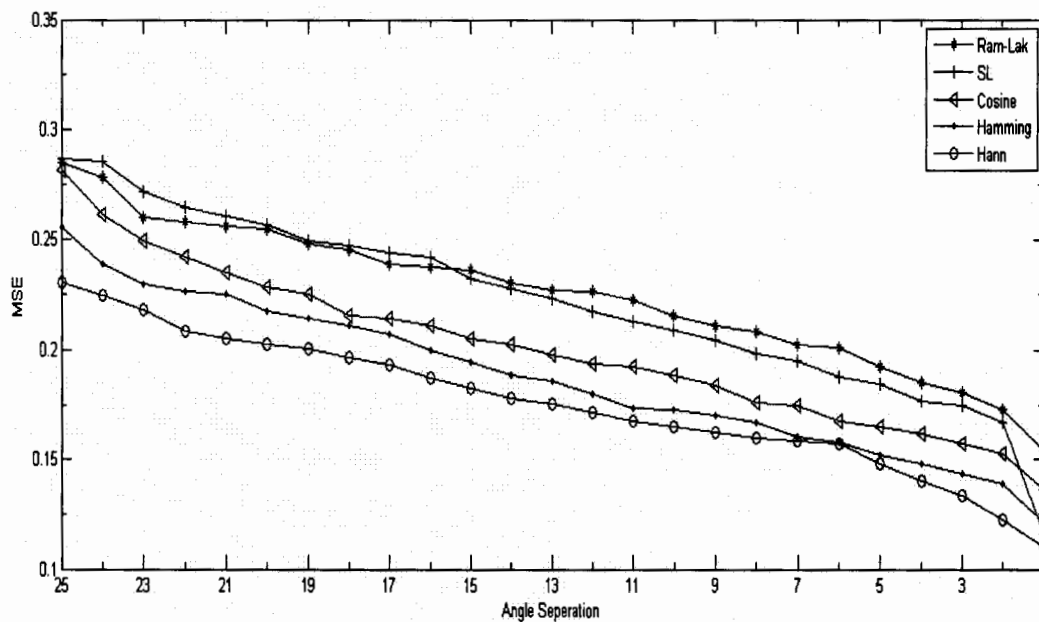
Additive noise is random in nature so it can be observed by visualization of images that the results are slightly bad as compare to the results of FBP algorithm having no channel response. As the variance or noise increases the results become poor in visualization. Table 5.3 shows the results of MSE for different angle separation for different filter types. It can be observed that from the table that MSE of deconvolution algorithm is also slightly more as compare to simple filtered back projection algorithm having ideal channel response and noise variance is zero.



**Table 5.2: MSE of Deconvolution Algorithm for channel known**

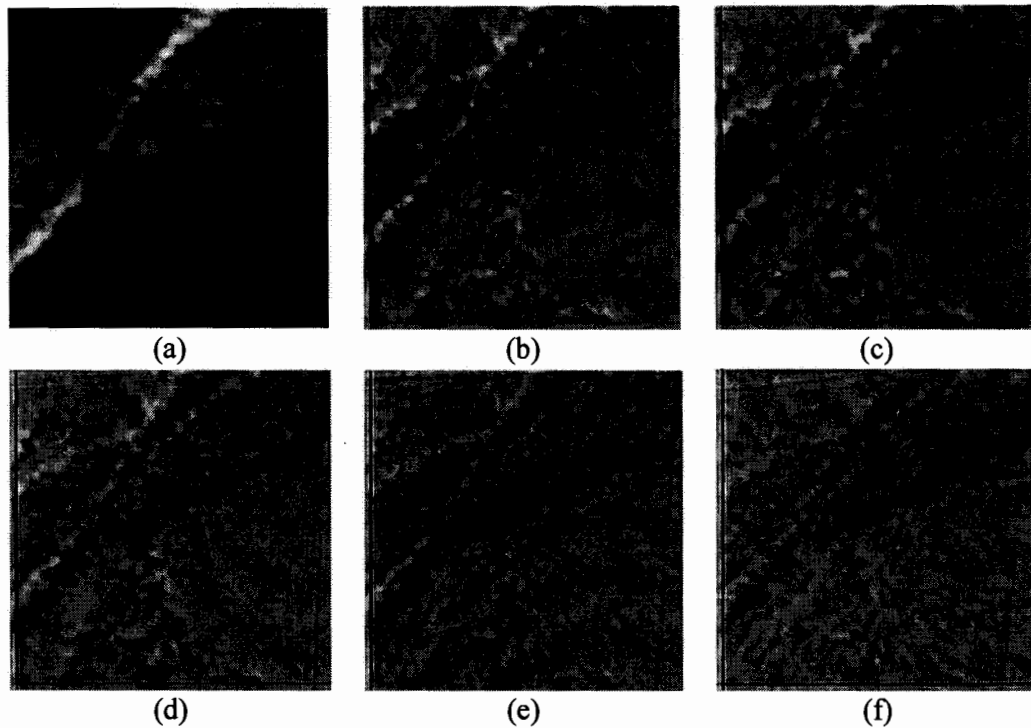
Filter	Theta=1	Theta=2	Theta=3	Theta=4	Theta=5
<b>Ram-Lak</b>	0.1539	0.1732	0.1805	0.1860	0.1928
<b>Shepp Logan</b>	0.1162	0.1671	0.1749	0.1766	0.1845
<b>Cosine</b>	0.1363	0.1525	0.1574	0.1617	0.1654
<b>Hamming</b>	0.1216	0.1319	0.1434	0.1481	0.1523
<b>Hann</b>	0.1099	0.1224	0.1334	0.1404	0.1479

Figure 5.4 shows the graph of MSE versus angle separation for different filters in deconvolution algorithm when channel response is completely known.



**Figure 5.4: Mean Square Error (MSE) versus Angle separation for different filters in deconvolution algorithm when channel response is completely known.**

Figure 5.5 shows the results of Deconvolution algorithm when channel is completely unknown and SNR is kept at 20dB. It can be observed that as the number of projection increases the results become quite good and vice versa.



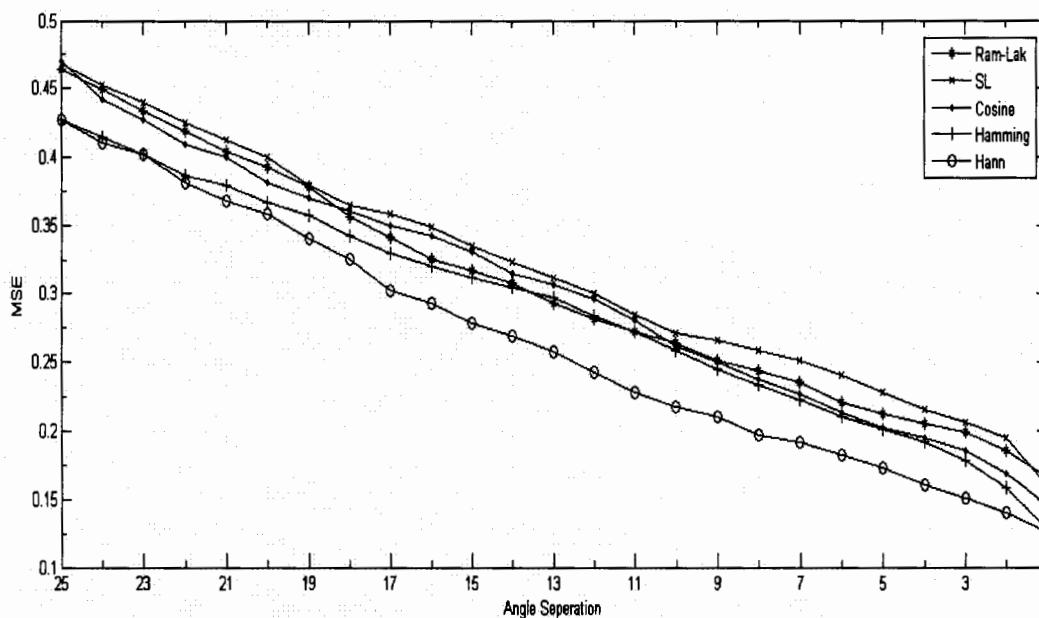
**Figure 5.5: (a) Original image for Deconvolution algorithm (Response Unknown) (b) Reconstruction using 180 projections (c) Reconstruction using 90 projections (d) Reconstruction using 60 projections (e) Reconstruction using 45 projections (f) Reconstruction using 36 projections.**

Table 5.3 shows the results of MSE of original and reconstructed image, when response of ultrasonic transducer is completely unknown and SNR is 20dB. If response of ultrasonic transducer is completely unknown the quality of reconstructed image becomes quite poor. Moreover the additive noise is also unknown and random in nature that results in poor results. The variance of additive noise plays an important role in degradation of image quality.

**Table 5.3: MSE of Deconvolution Algorithm for channel unknown**

Filter	Theta=1	Theta=2	Theta=3	Theta=4	Theta=5
<b>Ram-Lak</b>	0.1653	0.1855	0.1988	0.2057	0.2123
<b>Shepp Logan</b>	0.1589	0.1951	0.2063	0.2158	0.2281
<b>Cosine</b>	0.1455	0.1681	0.1853	0.1943	0.2022
<b>Hamming</b>	0.1273	0.1584	0.1783	0.1914	0.2012
<b>Hann</b>	0.1259	0.1404	0.1508	0.1601	0.1727

Figure 5.6 shows the graph of MSE versus angle separation for different filters in deconvolution algorithm when channel response is completely unknown.



**Figure 5.6: Mean Square Error (MSE) versus Angle separation for different filters in deconvolution algorithm when channel response is completely unknown.**

### 5.1.3 Wavelet based image reconstruction

The results of wavelet based filtered back projection algorithm is shown in this section for different values of angle separation. The quality of reconstructed image is quite good as compare to FBP and deconvolution algorithm. This algorithm is based on wavelet approach that works well even if the projections detected by ultrasonic detectors are not in their actual form i.e. noise or other artifacts. Noise variance plays an important role in image quality reconstructed from this algorithm, as with increase in noise variance the quality of reconstructed image becomes poor and poor as in other algorithms. Figure 5.7 shows results for wavelet based image reconstruction.

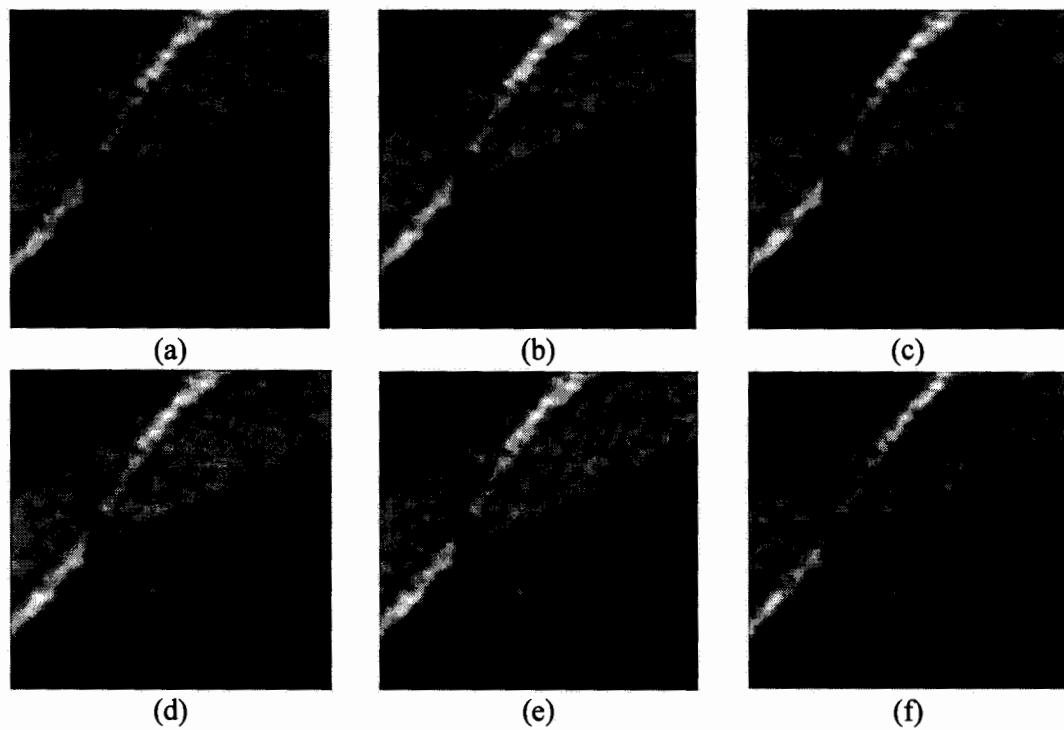
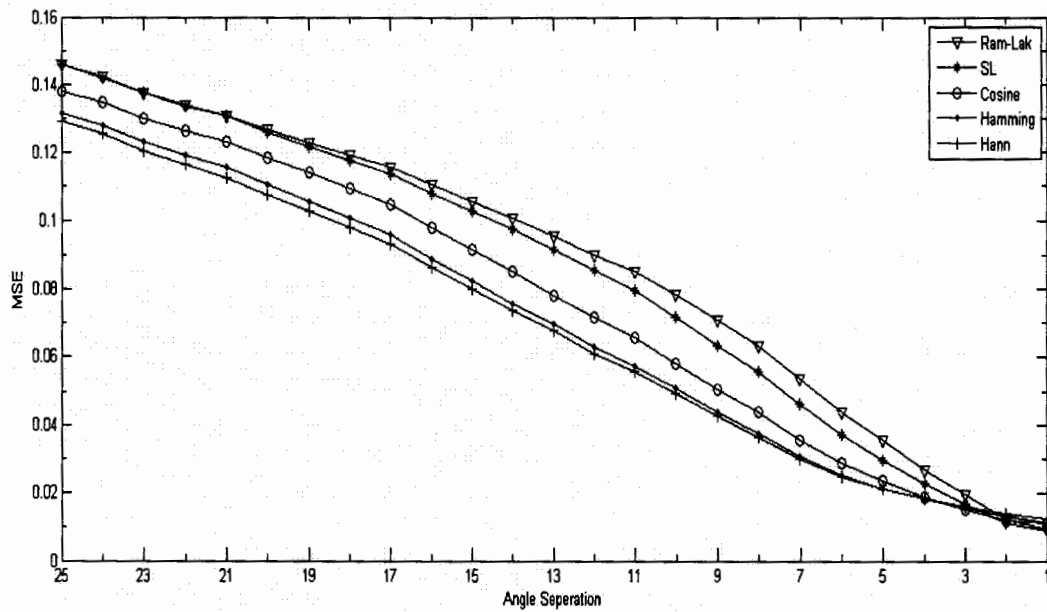


**Figure 5.7: (a) Original image for wavelet based image reconstruction (b) Reconstruction using 180 projections (c) Reconstruction using 90 projections (d) Reconstruction using 60 projections (e) Reconstruction using 45 projections (f) Reconstruction using 36 projections.**

Table 5.4 shows the MSE of original image and image reconstructed by mFBP algorithm for different values of angle separation.

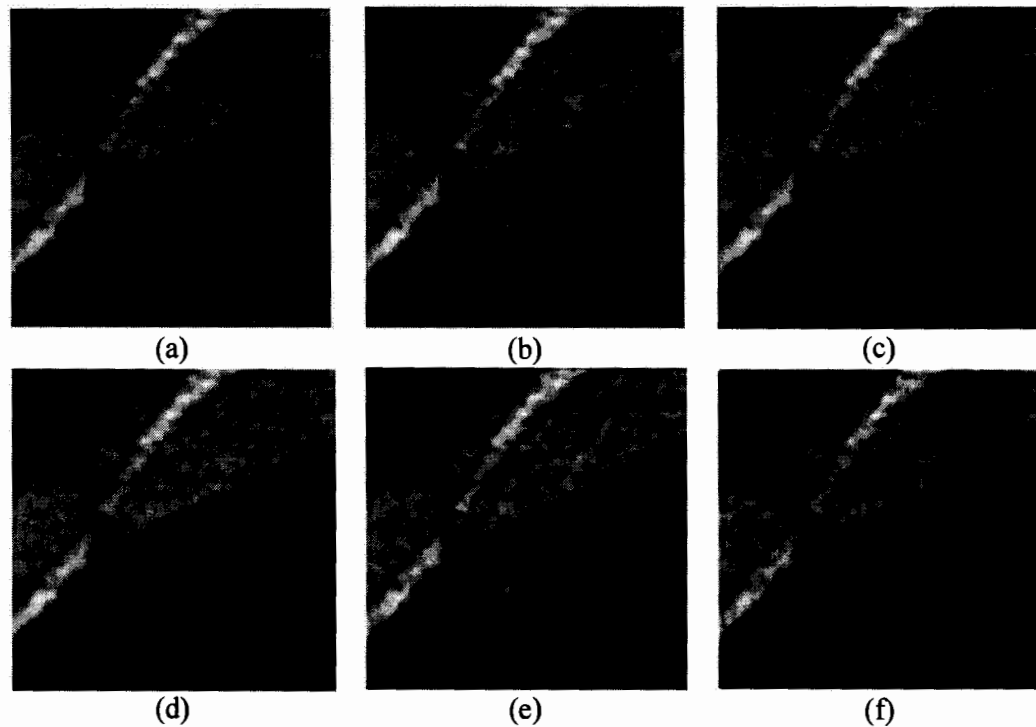
**Table 5.4: MSE of reconstructed (using mFBP) and original image**

Filter	Theta=1	Theta=2	Theta=3	Theta=4	Theta=5
<b>Ram-Lak</b>	0.0094	0.0106	0.0174	0.0258	0.0352
<b>Shepp Logan</b>	0.0089	0.0108	0.014	0.0215	0.029
<b>Cosine</b>	0.0112	0.0112	0.0138	0.0188	0.022
<b>Hamming</b>	0.0114	0.0131	0.0154	0.0188	0.0191
<b>Hann</b>	0.0123	0.0141	0.0159	0.0187	0.019



**Figure 5.8: Mean Square Error (MSE) versus Angle separation for different filters in modified wavelet based FBP algorithm.**

Figure 5.8 shows the graph of MSE versus angle separation for mFBP algorithm. Wavelet based deconvolution algorithm for channel impulse response completely known is shown in figure 5.9. Signal to noise ratio is kept at 20dB and ultrasonic or channel response is invariant or time. Result of wavelet based deconvolution algorithm is quite good as compare to simple deconvolution algorithm.



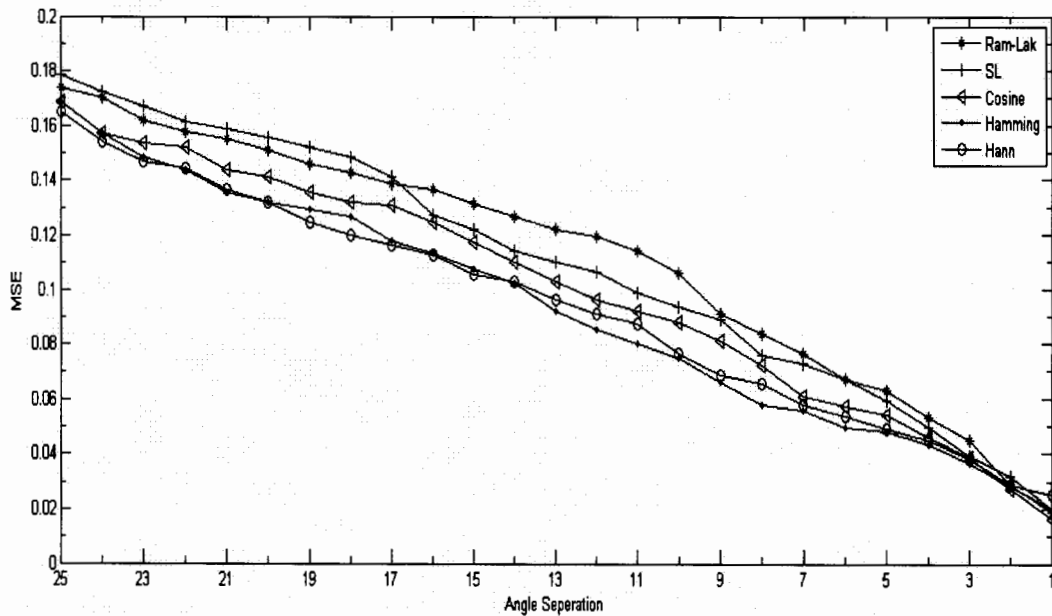
**Figure 5.9: (a) Original image for Wavelet based Deconvolution (Channel Known) mFBP algorithm (b) Reconstruction using 180 projections (c) Reconstruction using 90 projections (d) Reconstruction using 60 projections (e) Reconstruction using 45 projections (f) Reconstruction using 36 projections.**

Table 5.5 shows the MSE of original image and image reconstructed using wavelet based deconvolution mFBP algorithm for different values of angle separation and for different filter types. Increase in the number of projections results in less MSE and enhancement of image quality.

**Table 5.5: MSE of reconstructed Wavelet based deconvolution (channel known) mFBP algorithm.**

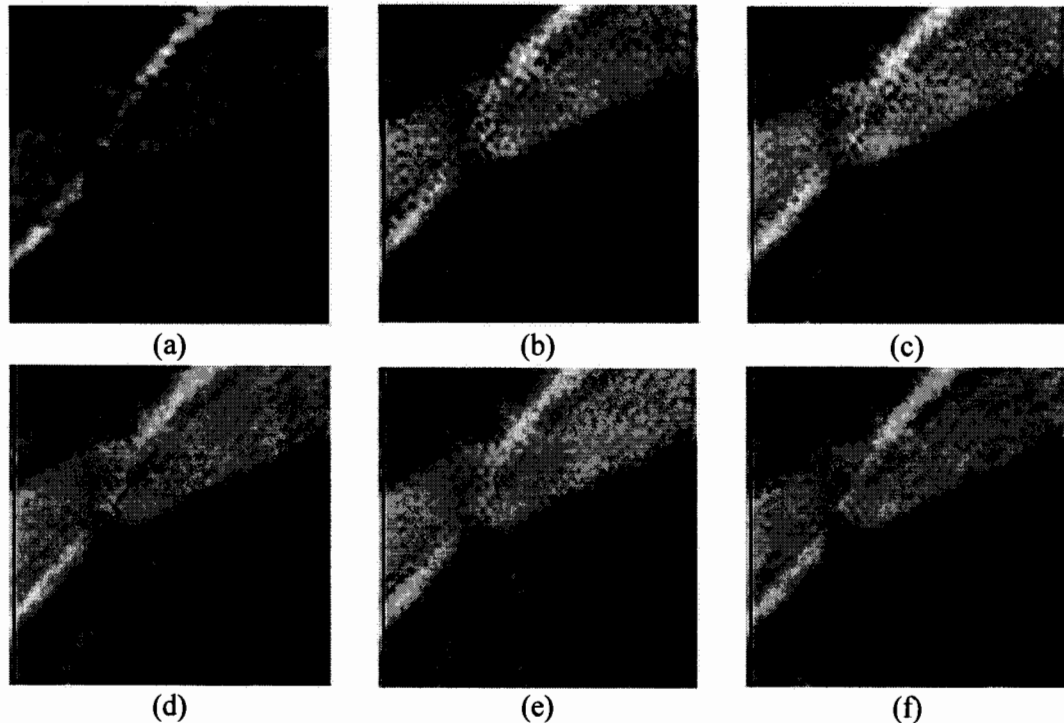
Filter	Theta=1	Theta=2	Theta=3	Theta=4	Theta=5
Ram-Lam	0.01913	0.02879	0.04464	0.05316	0.06295
Shepp Logan	0.02	0.03162	0.03936	0.04992	0.05934
Cosine	0.0165	0.02746	0.03844	0.04578	0.05409
Hamming	0.02018	0.02827	0.0366	0.04349	0.04785
Hann	0.02487	0.02855	0.0382	0.04498	0.04912

Figure 5.10 shows the graph of MSE versus angle separation for different filters in wavelet based deconvolution mFBP algorithm for channel completely known.



**Figure 5.10: Mean Square Error (MSE) versus Angle separation for different filters in wavelet based deconvolution algorithm when channel response is completely known.**

The graph shows that if the angle separation is less all the filters almost give same MSE but increase in number of projections result in different MSE for different filters. Wavelet based deconvolution algorithm for channel impulse response completely unknown is presented in figure 5.11. Result of wavelet based deconvolution algorithm is quite good as compare to simple deconvolution algorithm.



**Figure 5.11: (a) Original image for wavelet based deconvolution algorithm for channel completely unknown (b) Reconstruction using 180 projections (c) Reconstruction using 90 projections (d) Reconstruction using 60 projections (e) Reconstruction using 45 projections (f) Reconstruction using 36 projections.**

Table 5.6 shows the MSE of original image and image reconstructed using wavelet based deconvolution (channel unknown) mFBP algorithm for different values of angle separation and for different filter types. Increase in the number of projections results in less MSE and enhancement of image quality.



**Table 5.6: MSE of reconstructed image using Wavelet based deconvolution (Unknown) mFBP algorithm.**

Filter	Theta=1	Theta=2	Theta=3	Theta=4	Theta=5
Ram-Lak	0.06046	0.08835	0.1142	0.1264	0.1363
Shepp Logan	0.04954	0.07429	0.1068	0.1163	0.1381
Cosine	0.05692	0.07921	0.1019	0.1096	0.1148
Hamming	0.06268	0.07017	0.0826	0.1082	0.1126
Hann	0.04767	0.06933	0.09374	0.1063	0.1144

Figure 5.12 shows the graph of MSE versus angle separation in wavelet based deconvolution mFBP algorithm for channel completely unknown. The graph shows that increase in number of projections result in different MSE for different filters.

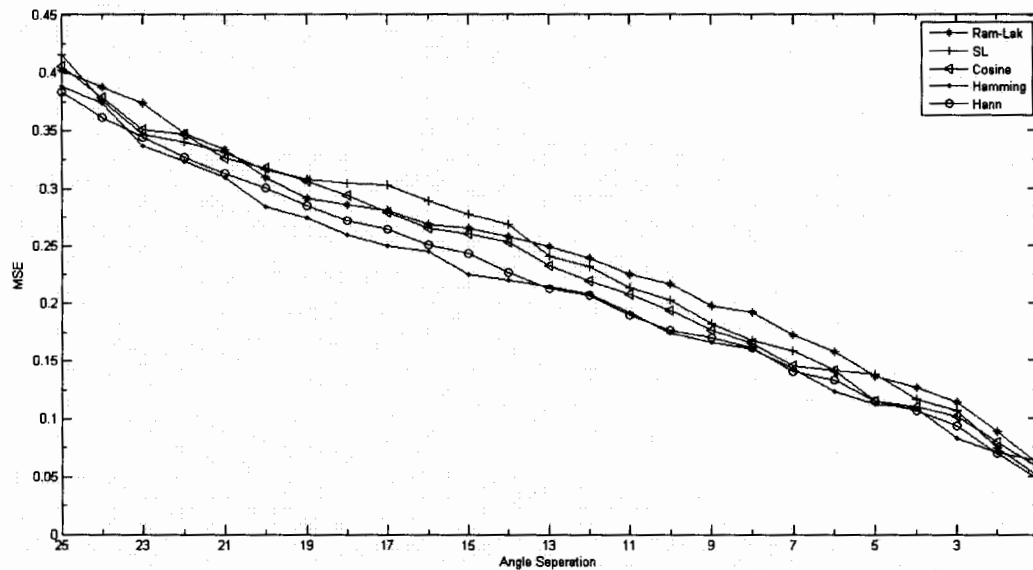


**Figure 5.12: Mean Square Error (MSE) versus Angle separation for different filters in wavelet based deconvolution algorithm mFBP when channel response is completely unknown.**

### 5.1.4 Comparison of Different Algorithms

Comparison of different algorithms is presented in this section. Table 5.7 shows the results of Filtered back projection and modified Filtered back projection algorithm in terms of ISNR (Improved SNR). As the value of 'Theta' increases, the number of projection decreases and quality of image reconstructed using FBP decreases, while on the other hand the quality of image reconstructed using mFBP is comparable with that of original image. ISNR is the ratio of two MSE, as the difference of two MSE become high the valued of ISNR become high and vice versa.

**Table 5.7: ISNR of FBP and wavelet based mFBP**

<b>Filter</b>	<b>Theta=1</b>	<b>Theta=2</b>	<b>Theta=3</b>	<b>Theta=4</b>	<b>Theta=5</b>
<b>Ram-Lam</b>	2.1648	2.4127	2.1873	1.9787	1.8331
<b>Shepp Logan</b>	2.0479	2.397	2.3095	2.081	1.9451
<b>Cosine</b>	1.6498	2.161	2.1413	2.0014	1.985
<b>Hamming</b>	1.5143	1.9113	1.9815	1.9103	1.9576
<b>Hann</b>	1.4213	1.7894	1.877	1.8235	1.8626

Figure 5.13 shows the results of MSE for FBP and mFBP for different value of angle separation. It can be observed that MSE of FBP algorithm is slightly more as compare to wavelet based mFBP algorithm.

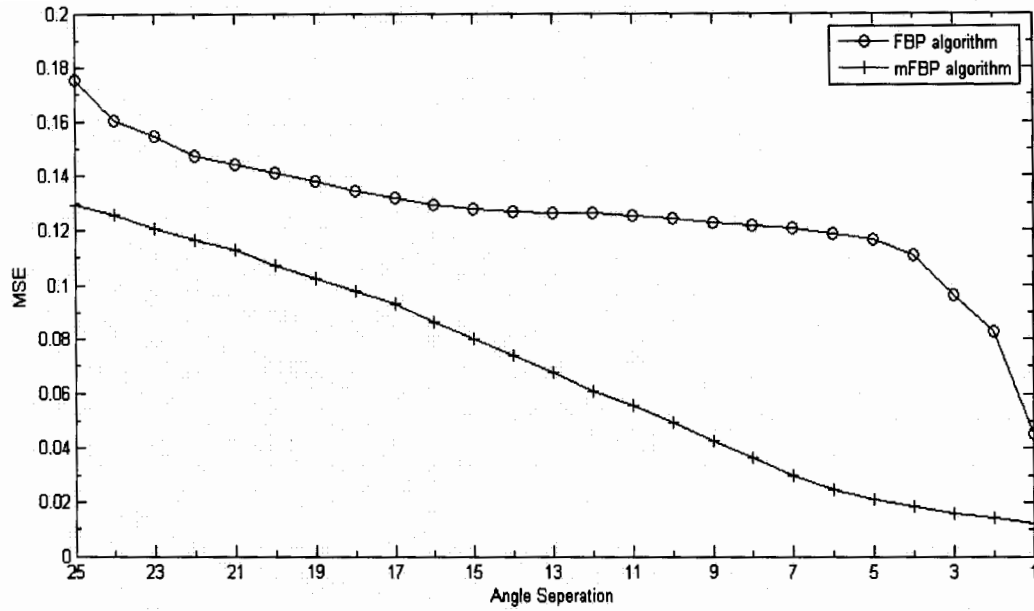


**Figure 5.13: Mean Square Error (MSE) versus Angle separation for FBP and mFBP algorithm.**

Table 5.8 shows the results of deconvolution algorithm for channel completely known based on FBP and mFBP techniques in terms of ISNR.

**Table 5.8: ISNR for FBP and mFBP Deconvolution Algorithm (Channel Known)**

Filter	Theta=1	Theta=2	Theta=3	Theta=4	Theta=5
<b>Ram-Lam</b>	2.1141	2.0234	1.8161	1.7446	1.68
<b>Shepp Logan</b>	1.8175	1.9305	1.8554	1.7287	1.6712
<b>Cosine</b>	2.0595	1.9116	1.7624	1.6926	1.6212
<b>Hamming</b>	1.8524	1.7603	1.7031	1.6416	1.6152
<b>Hann</b>	1.6729	1.693	1.6208	1.5798	1.5767

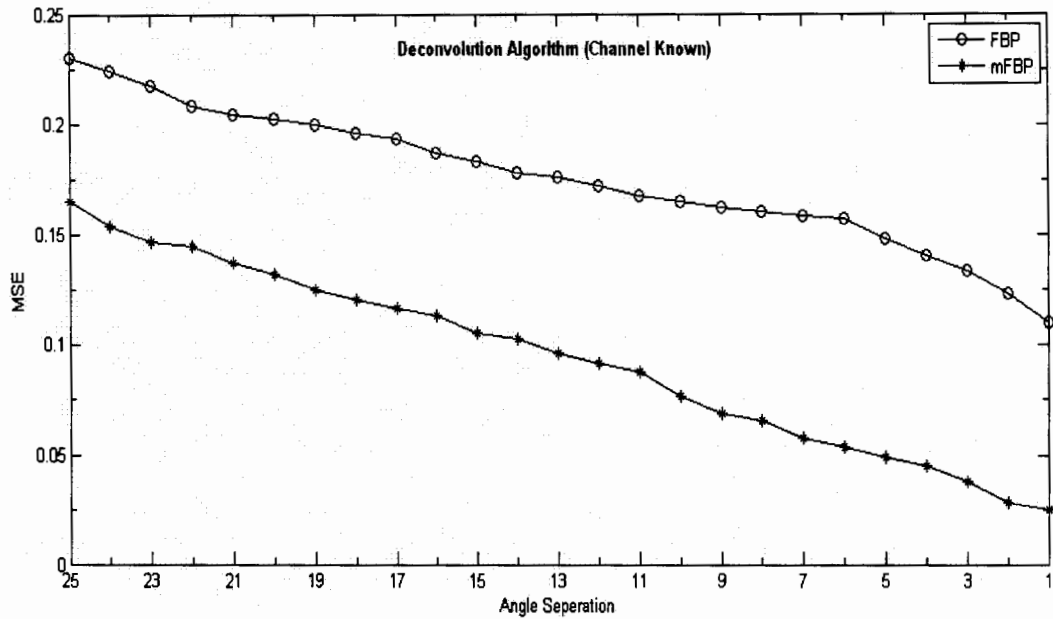


**Figure 5.14: Mean Square Error (MSE) versus Angle separation for Deconvolution (Channel known) FBP and mFBP algorithm.**

Figure 5.14 shows MSE graph for FBP and mFBP deconvolution (channel known) algorithms for different values of angle separation.

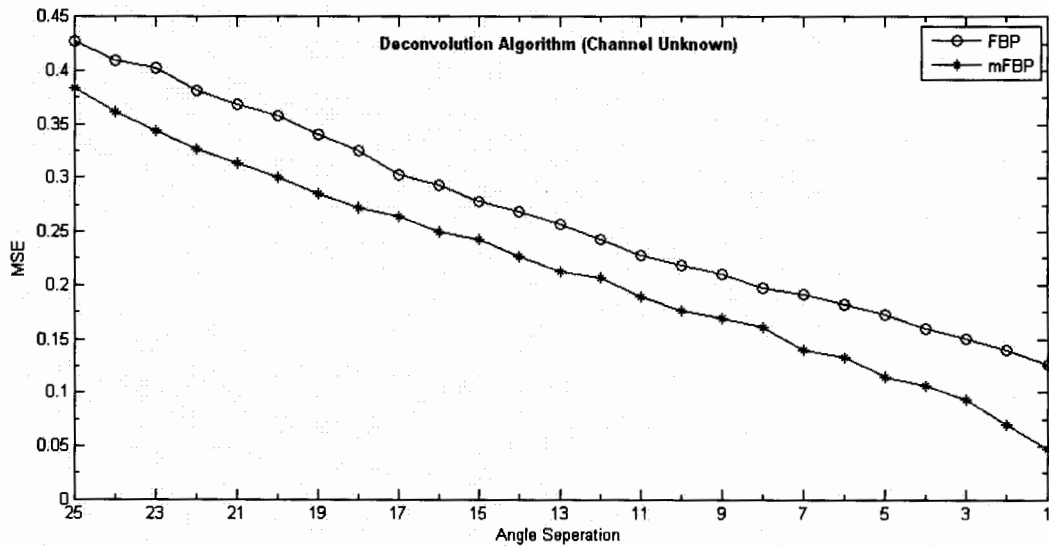


**Figure 5.15: Mean Square Error (MSE) versus Angle separation for Deconvolution (Channel unknown) FBP and mFBP algorithm.**

Figure 5.15 shows the results of MSE for deconvolution (channel unknown) FBP and mFBP algorithms for different value of angle separation. Table 5.9 shows the results of deconvolution algorithm for channel completely unknown based on FBP and mFBP techniques in terms of ISNR.

**Table 5.9: ISNR for FBP and mFBP Deconvolution (Unknown) Algorithm.**

<b>Filter</b>	<b>Theta=1</b>	<b>Theta=2</b>	<b>Theta=3</b>	<b>Theta=4</b>	<b>Theta=5</b>
<b>Ram-Lam</b>	1.5588	1.4403	1.3432	1.3079	1.2859
<b>Shepp Logan</b>	1.6336	1.5908	1.4171	1.4031	1.3395
<b>Cosine</b>	1.4869	1.422	1.3547	1.3495	1.3541
<b>Hamming</b>	1.3437	1.4419	1.4462	1.345	1.362
<b>Hann</b>	1.4687	1.3594	1.2513	1.2235	1.2345

In nutshell it can be observed that wavelet based algorithms provides better results as compare to other algorithms. ISNR and MSE graph shows that mFBP algorithm provides almost double accuracy as compare to FBP. Moreover the results of Hann filter are better as compare to other filters. In deconvolution algorithm if the noise variance increases the results become poor even if the channel is know. If channel is unknown in Deconvolution algorithm than almost all the filters provide same results in terms of MSE.

## 5.2 Color Quantization Results

Results of uniform quantization and quantization using SOM are concluded in this section. Figure 5.16 shows the results of color quantization using uniform quantization technique.

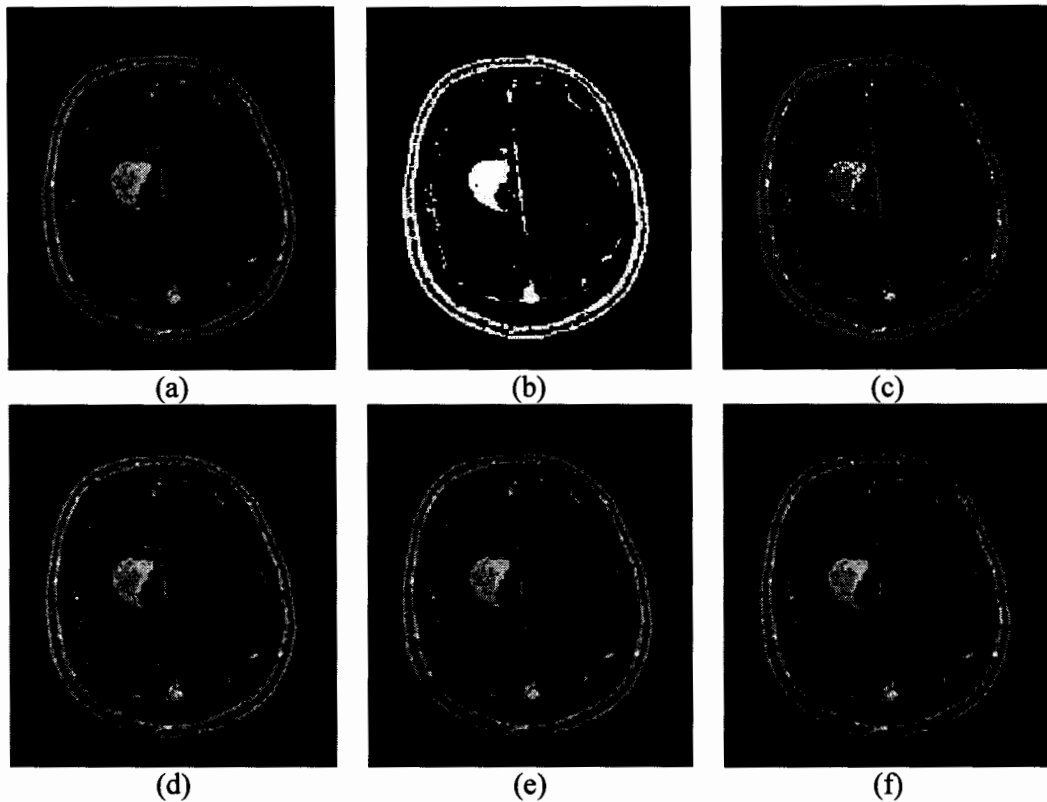


**Figure 5.16: (a) Original image for uniform quantization (b) Quantized image 2 colors (c) Quantized image 4 colors (d) Quantized image 8 colors (e) Quantized image 16 colors (f) Quantized image 32 colors.**

It can be observed that as the number of colors increases the quality of quantized image increases. As the colors are greater in number so the quality in above mention figure is quite good and can be comparable with quality of original image.

Results of median cut quantization are given in figure 5.17. Median cut color quantization is based on image histogram. The resultant quantized image from this technique has better quality as compare to uniform quantized image.

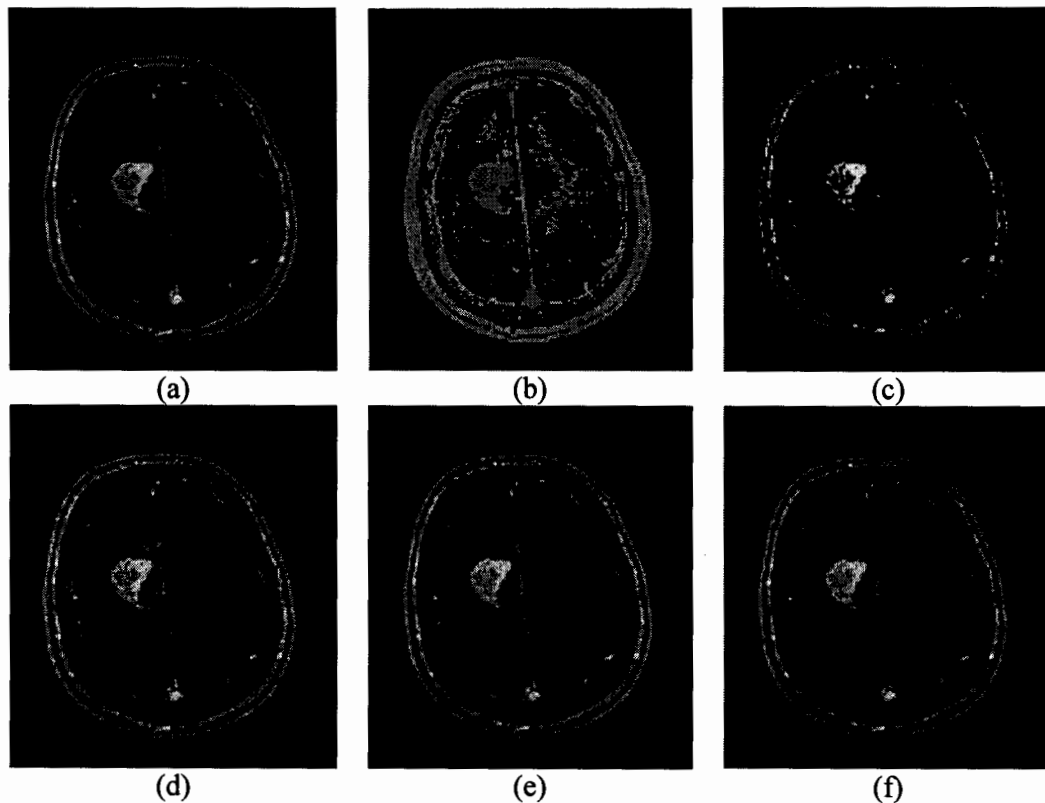


**Figure 5.17: (a) Original image for median cut quantization (b) Quantized image 2 colors (c) Quantized image 4 colors (d) Quantized image 8 colors (e) Quantized image 16 colors (f) Quantized image 32 colors.**

Color quantization using SOM is shown by figure 5.18 for different color levels. SOM is neural network based color quantization technique so it gives better results even if image histogram is not uniform.

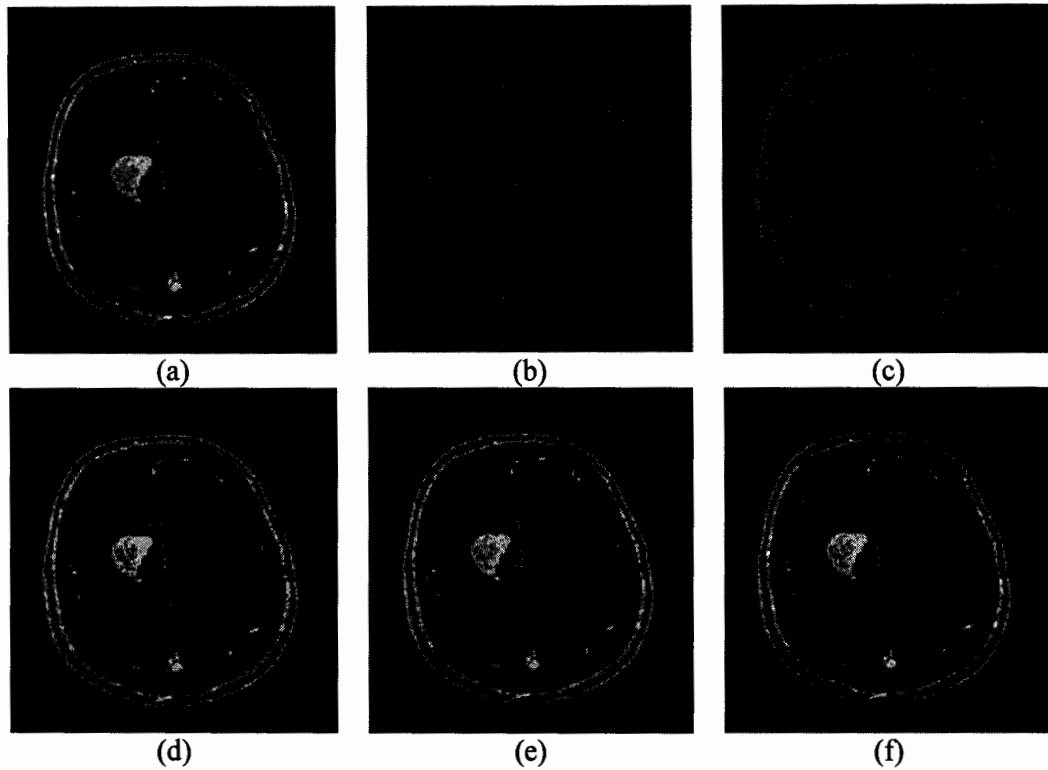


**Figure 5.18: (a) Original image for SOM quantization (b) Quantized image 2 colors (c) Quantized image 4 colors (d) Quantized image 8 colors (e) Quantized image 16 colors (f) Quantized image 32 colors.**

Results of uniform and SOM quantization may be comparable as the numbers of color are more in number. Results of quantization techniques are summarized in table 5.10.

**Table 5.10: MSE for different color quantization schemes.**

<b>MSE vs. color</b>	<b>N=2</b>	<b>N=4</b>	<b>N=8</b>	<b>N=16</b>	<b>N=32</b>
<b>Uniform</b>	0.1608	0.0590	0.0173	0.0134	0.0034
<b>Median Cut</b>	0.1128	0.0297	0.0296	0.0085	0.0022
<b>SOM</b>	0.0445	0.0304	0.0050	0.0023	0.0012
<b>Size reduction</b>	87.5%	75%	62.5%	50%	37.5%

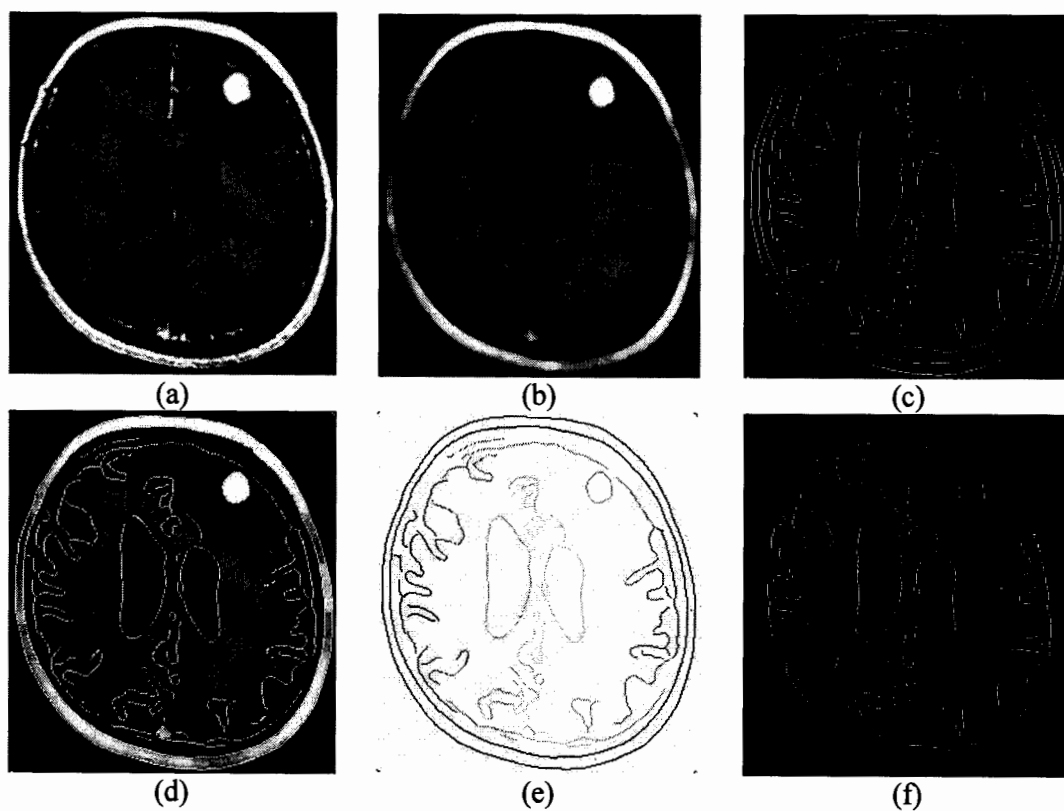


### 5.3 Results of Segmentation and Classification

Results of both segmentation and classification are discussed in this section for proposed algorithms.

#### 5.3.1 Single level Segmentation and Classification

The result of proposed single level segmentation and classification technique is shown by figure 5.19.



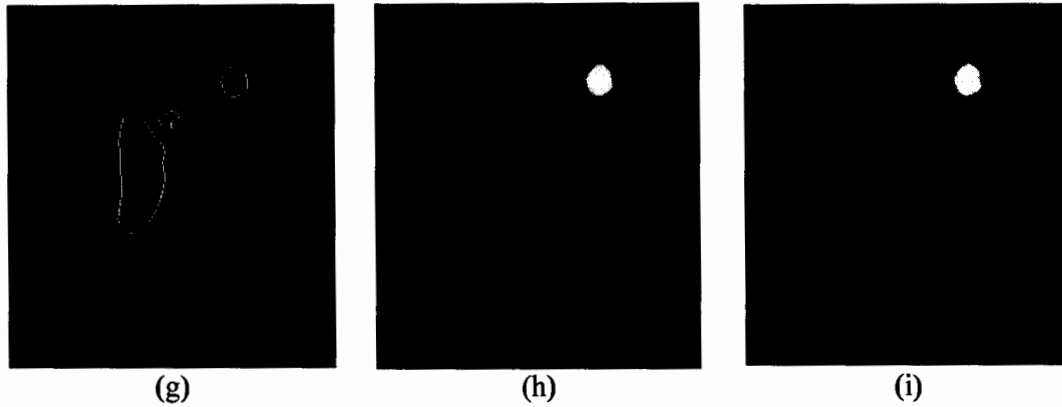


**Figure 5.19: (a) Original Image (b) Median Filtered image (c) Edges of filtered image (d) Edge + Filtered Image (e) Labeled Edge (f) Medium size edges (g) Closed Edges (h) All segments detected (i) ROI image.**

Single level segmentation and classification as discussed in chapter 4 is one of the proposed segmentation and classification technique. As shown in figure 5.19 we have three resultant segments and we have to classify them in either tumor or non-tumor regions.

**Table 5.11: Average intensity of region and absolute difference with Mean of image (Average intensity on image is 106.4197)**

Segment Number	Average intensity of segments	Absolute difference of segment intensities with mean
1	73.9663	32.4534
2	113.1000	6.6803
3	243.4386	137.0189

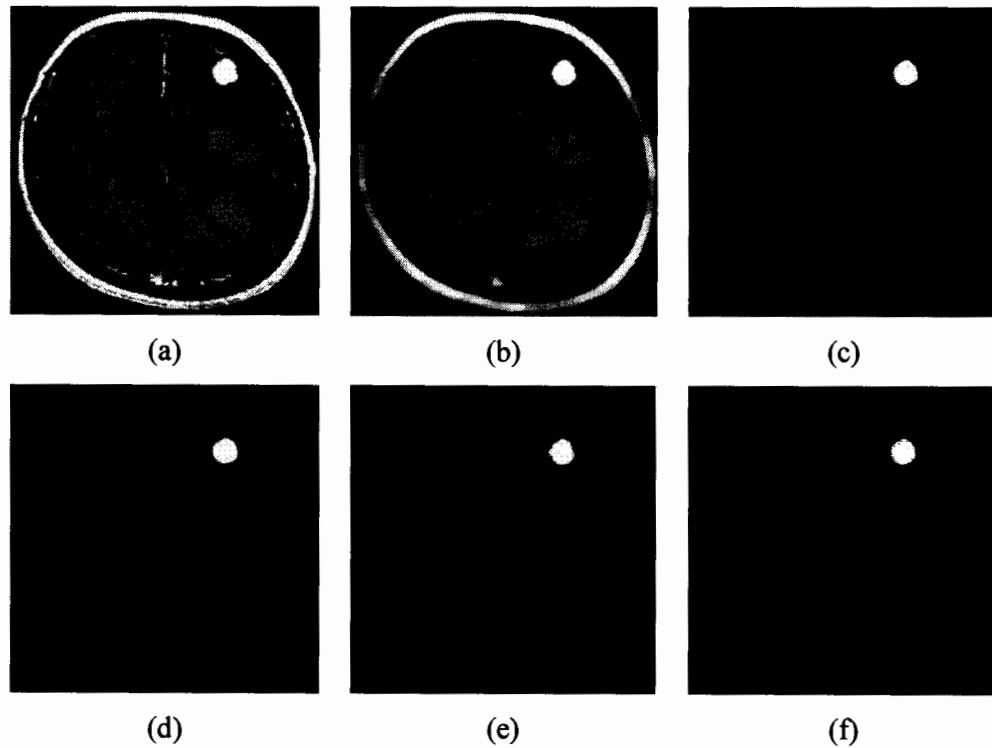
Table 5.11 shows the average intensity value of whole image and average intensity values of segmented regions ad their absolute differences. It can be easily seen that

third segment has maximum absolute difference as compare to other segments. As due to unavailability of PAT images the algorithm is tested on MRI images. This

algorithm can be applied on PAT images without any major modifications and results on PAT images will be quite good as compare to MRI images. This segmentation technique is faster as compare to other segmentation techniques but sometimes if the image quality is poor this technique may not provide good segmentation and classification results.

### 5.3.2 Multilevel Segmentation and Classification

Figure 5.20 shows the results of proposed multilevel segmentation and classification technique.



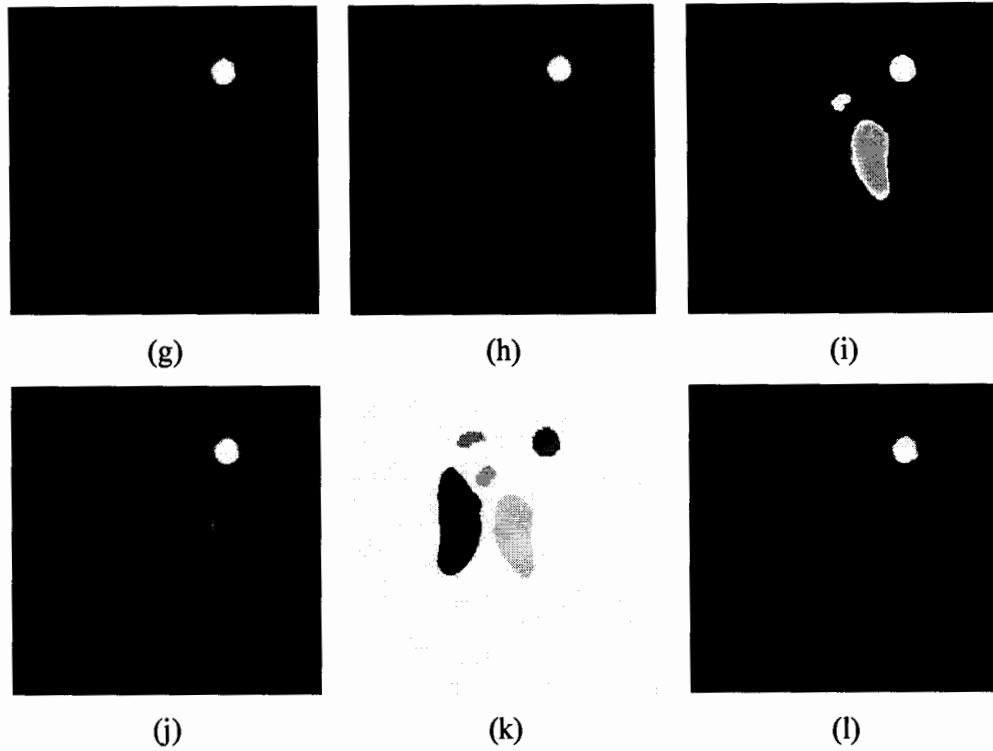


**Figure 5.20: (a) Original image (b) Filtered Image (c) Segments of Original image (d) Segments of 0.9 scale image (e) Segments of 0.8 scale image (f) Segments of 0.7 scale image (g) Segments of 0.6 scale image (h) Segments of 0.5 scale image (i) Addition of all segments (j) Respective segments form original image (k) labeled segments (l) Resultant ROI**

**Table 5.12: Average Intensity of region and absolute difference with mean of image (Average intensity on image is 108.0012)**

<b>Region Number</b>	<b>Average intensity of Region</b>	<b>Absolute difference of region intensities with mean</b>
1	73.9663	34.0349
2	110.7636	2.7624
3	116.8406	8.8394
4	81.0261	26.9751
5	229.9761	121.9749

It can be seen from figure 5.20 that multilevel edge detector detects more segments as compare to single level edge detection scheme making it more reliable scheme for edge detection and classification. Table 5.13 shows the results of PCC for single level segmentation and classification (SLSC) and multilevel segmentation and classification (MLSC).

**Table 5.13: Average Intensity of region and absolute difference with Mean of image (Average intensity on image is 108.0012)**

<b>Algorithm Type</b>	<b>Percentage of Correct Classification</b>	<b>Percentage of Incorrect Classification</b>
<b>SLSC</b>	82.5%	17.5%
<b>MLSC</b>	93%	7%

It can be observed by Table 5.13 that percentage of correct classification is more in Multilevel segmentation and classification technique as compare to single level segmentation and classification because of the fact that segmentation is done more elegantly in MLSC as compare to SLSC.

## **CHAPTER 6**

### **CONCLUSION AND FUTURE DIRECTIONS**

The applications of PAT in medical imaging give many challenging research and development problems in many areas. Algorithms used for image reconstruction and classification should be improved to fully enjoying the features of PAT.

#### **6.1 Summary of Results**

A general introduction of PAT is discussed in chapter 1. In chapter 2, basics of medical imaging techniques that use tomography principle are discussed.

In chapter 3, brief introduction of PAT is discussed. Inverse problem in PAT imaging is derived from basic acoustic and thermal equations. The detection techniques are also discussed in this chapter. Image reconstruction, one of the most challenging and hot area of research in PAT is also discussed in this chapter. Three different

algorithms are used in this thesis for image reconstruction i.e. Filtered back projection, Deconvolution algorithm and Modified filtered back projection algorithm. Mathematical basis of these algorithms are also derived in chapter 3. In chapter 4, the classification problem in PAT is discussed. PAT image color quantization using uniform color quantization technique, median cut color quantization technique and SOM color quantization technique. Novel segmentation and classification technique is also proposed in this chapter.

In chapter 5, the simulation results of PAT image reconstruction and classification is discussed. PAT image quality is directly dependent on the reconstruction algorithm used. Filtered back projection algorithm is used for image reconstruction when ultrasonic response is ideal. Deconvolution algorithm is used when the response of ultrasonic transducer is not ideal. Additive white Gaussian noise of zero mean and various intensities are used for evaluating performance of algorithms. Modified filtered back projection algorithm is also used for noise suppression and image enhancement. Color quantization using uniform quantization algorithm, median cut color quantization and SOM color quantization are also used for memory detection and segmentation purpose. Novel segmentation and classification approach are proposed that gives comparable results as compare to other techniques.

## **6.2 Future Directions**

PAT is a novel medical imaging technique that gives many opportunities in terms of research and development; some of them are listed as under:

- Performance evaluation of PAT exact reconstruction and approximate reconstruction can be done in future.
- Genetic Algorithms (GA) and Particle swarm optimization (PSO) techniques can be used for PAT image reconstruction.
- New features can be proposed for PAT image classification in terms of ROI.
- Proposed segmentation technique can be improved to get much better results.
- Deconvolution algorithm can also be modified for unknown response of ultrasonic response.



## Reference

- [1]. M. Xu and L. V. Wang, "Photoacoustic imaging in biomedicine", 2006, American Ins. Phys. 10.1063/1.2195024.
- [2]. Jeri Jan, "Medical image processing reconstruction and restoration", CRC press, 2006.
- [3]. L.V.Wang, X.Wang, Y.Xu, M.Xu, S.Yokoo and E.S.Fry, "Photoacoustic tomography of biological tissues with high cross-section resolution: Reconstruction and experiment," *Med. Phy*, vol. 29, no. 12, 2002.
- [4]. Lena Costaridou "Medical imaging analysis method", CRC press, 2005.
- [5]. R.O. Esenaliev, A. A. Karabutov and A. A. Oravsky, "Sensitivity of laser optoacoustic imaging in detection of small deeply embedded tumors", *IEEE J Sel Top Quant* 5(1999), 981-988.

- [6]. A. Beenen, G. Spanner and R. Niessner, "Photoacoustic depth-resolved analysis of tissue models", *Appl Spectrosc* 51(1997), 51-57.
- [7]. C. G. A. Hoelen, F. F. M. de Mul, R. Pongers and A. Dekker, "Three-dimensional photo-acoustic imaging of blood vessels in tissue", *Opt. Lett* 23 (1998) 648-650.
- [8]. G. Paltauf and H. Schmidt-Kloiber, "Optical method for two-dimensional ultrasonic detection" *Appl Phys Lett* 75 (1999), 1048-1050.
- [9]. K. P. Kostili, D. Frauchiger, J.J. Niederhauser, G. Paltauf, H. P. Weber and M. Frenz, "Opto-acoustic imaging using a three-dimensional reconstruction algorithm", *IEEE JSel Top Quant* 7 (2001), 981-923.
- [10]. M. H.. Xu, G. Ku and L. H. V. Wang, "Microwave-induced thermo-acoustic tomography using multi-sector scanning", *Med Phys* 28 (2001), 1958-1963.
- [11]. R. A. Kruger, P. Liu, Y. R. Fang and C. R. Appledorn, "Photoacoustic ultrasound (PASU)- reconstruction tomography", *Med Phys* 22 (1995), 1605-1609.
- [12]. K. Kostli, M. Fernz, H. Bebie and H. Weber, "Temporal backward projection of opto-acoustic pressure transients using Fourier transform methods", *Phys Med Biol* 46 (2001), 1863-1872.

- [13]. P. Beard “Photoacoustic imaging of blood vessel equivalent phantoms” SPIE 4618, pp 54-62, 2002.
- [14]. M Xu and L. V. Wang “Universal back projection algorithm for Photoacoustic computed tomography” American Physical Society 2005, 016706(1-7).
- [15]. Y. Xu, D. Feng and L. V. Wang, “Exact frequency domain Reconstruction for thermoacoustic tomography: I. Planar geometry” IEEE, Med. Img. 21 (7) 2002.
- [16]. Y. Xu, D. Feng and L. V. Wang, “Time domain reconstruction for thermoacoustic tomography in spherical geometry” IEEE, Med. Img. 21 2002.
- [17]. Y. Xu, D. Feng and L. V. Wang, “Exact Frequency Domain Reconstruction for thermoacoustic tomography: II. Cylindrical geometry” IEEE, Med. Img. 21 (7) 2002.
- [18]. Y. Wang, D. Xing, Y. Zeng and Q. Chen “Photoacoustic Imaging with deconvolution Algorithm” Phys. Med. Biol 49 (2004) 3117-3124.
- [19]. L. Zeng, Guodong, B. Shao, Z. Ren and Z. Huang, “Image Reconstruction of high quality Photoacoustic tomography using wavelet-analysis-based algorithm”, IEEE, Med. Img. 2008.

- [20]. W. Joines, Y. Zhand, C. Li and R. Jirtle, "The measured electrical properties of normal and malignant human tissues from 50-500MHz" *Med. Phys.* 21, 1994.
- [21]. J. Zhang, M. A. Anastasio, X. Pan and L. V. Wang "Weighted expectation maximization reconstruction algorithm for thermoacoustic tomography" *IEEE Trans. Med. Imag.* Vol. 24, No 6, 2005
- [22]. G. Ku, X. Wang, G. Stoica and L. V. Wang, "Multiple bandwidth Photoacoustic tomography *Phys. Med. Biol.*, vol 49, pp. 1329-1338, 2004.
- [23]. S. Norton, "Reconstruction of a two dimensional reflecting medium over a circular domain: Exact solution", *J. Acoust. Soc. Amer.*, vol. 67, no. 4, pp. 1266-1273
- [24]. T. J. Allen, B. T. Cox and P. C. Beard, "Generating Photoacoustic signals using high peak power pulsed laser diodes" *SPIE 5696*, pp. 233-242, 2005.
- [25]. L. V. Wang, X. Wang, G. Ku, X. Xie, G. Stoica, "High resolution Photoacoustic tomography" *IEEE*, 2004.
- [26]. P. J. Riviere, J. Zhang and M. A. Anastasio, "Image reconstruction in optoacoustic tomography accounting for frequency dependent attenuation" *IEEE, Nucl. Sci. Symp.* 2005

- [27]. G. Ku and L. V. Wang, "Scanning thermoacoustic tomography in biological tissues", *Med Phys*, vol. 27, pp. 1195-1202, 2002.
- [28]. N. V. Sushilov and R. S. C. Cobbold, "Frequency domain wave equation and its time domain solutions in attenuating media", *J. Acoust. Soc. Am.*, vol. 115, pp. 1336-1347, 2001.
- [29]. H. F. Zhang, K. Maslov, G. Stoica and L. V. Wang, "Functional photoacoustic microscopy for high-resolution and noninvasive in vivo imaging". *Nature Biotechnology* 24: 848 – 851, 2006
- [30]. X. Wang, X. Xie, G. Ku, L. V. Wang and G. Stoica, "Non-invasive imaging of hemoglobin concentration and oxygenation in the rat brain using high-resolution photoacoustic tomography". *Journal of Biomedical Optics* 11(2): 024015, 2006
- [31]. X. Wang, X. Xie, G. Ku, L. V. Wang and G. Stoica, "Non-invasive laser-induced photoacoustic tomography for structural and functional imaging of the brain in vivo". *Nature Biotechnology* 21(7): 803-806, 2003
- [32]. X. Wang, X. Xie, G. Ku, L. V. Wang and G. Stoica "Thermoacoustic and photoacoustic tomography of thick biological tissues toward breast imaging". *Technology in Cancer Research and Treatment*, 559-566, 2005.

- [33]. V. Tuchin "Tissue Optics: Light Scattering Methods and Instruments for Medical Diagnosis" SPIE, 2007.
- [34]. Maslov K, Stoica G, Wang LVH. "In vivo dark-field reflection-mode photoacoustic microscopy" Optics Letters, 30(6), 625–627, 2005.

